nature biomedical engineering

Article

https://doi.org/10.1038/s41551-023-01142-x

Genetically encoding multiple functionalities into extracellular vesicles for the targeted delivery of biologics to T cells

Received: 28 April 2022

Accepted: 20 October 2023

Published online: 27 November 2023

Check for updates

Devin M. Stranford[1,2], Lacy M. Simons[3,4], Katherine E. Berman[2,5], Luyi Cheng[2,5], Beth N. DiBiase[1,2], Michelle E. Hung[2,5], Julius B. Lucks[1,2,5,6], Judd F. Hultquist[3,4] & Joshua N. Leonard[1,2,5,6,7]

The genetic modification of T cells has advanced cellular immunotherapies, yet the delivery of biologics specifically to T cells remains challenging. Here we report a suite of methods for the genetic engineering of cells to produce extracellular vesicles (EVs)—which naturally encapsulate and transfer proteins and nucleic acids between cells—for the targeted delivery of biologics to T cells without the need for chemical modifications. Specifically, the engineered cells secreted EVs that actively loaded protein cargo via a protein tag and that displayed high-affinity T-cell-targeting domains and fusogenic glycoproteins. We validated the methods by engineering EVs that delivered Cas9–single-guide-RNA complexes to ablate the gene encoding the C-X-C chemokine co-receptor type 4 in primary human $CD4^+$ T cells. The strategy is amenable to the targeted delivery of biologics to other cell types.

Genome engineering of human T cells mediated by clustered regularly interspaced short palindromic repeats (CRISPR)–Cas9 is an area of active investigation for the development of therapeutics to treat cancer, autoimmunity and infectious disease[1]. Delivery of the programmable nuclease Cas9 with a single guide RNA (sgRNA) complementary to a target sequence results in the introduction of double-stranded breaks that can introduce frameshift mutations in coding genes and the ablation of protein expression. Alternately, co-delivery of a homology-directed repair template can insert specified mutations, insertions or deletions into the genomes of target cells. While this technology has multiple applications, translation of this strategy remains difficult due to the challenges associated with in vivo delivery of Cas9. One approach that leverages foundational gene therapy advances is adeno-associated virus (AAV) vehicles, although safety and efficacy are often limited by anti-vector immunity and limited tissue tropism[2–6]. Virus-like particles can also deliver Cas9 nucleases or base editors[7–9], although it remains unclear whether the immunogenicity of viral proteins will likewise limit these approaches[10]. Synthetic nanoparticle–nucleic acid (for example, messenger RNA) delivery is an alternative to viral vectors and has been used for the in vivo delivery of mRNA to confer sustained expression of chimeric antigen receptors in murine T cells[11]. However, achieving efficient T-cell targeting in a manner that confers the transient expression of Cas9 needed to avoid off-target effects remains challenging[12,13]. These general difficulties are uniquely compounded by the challenge of delivering any cargo to T cells, which show low rates of endocytosis[14]. Altogether, there exists substantial opportunity to improve delivery systems that could enable delivery of biologics to T cells inside a patient.

A promising emerging strategy is the use of extracellular vesicles (EVs) to deliver biomolecular cargo. EVs are nanoscale, membrane-enclosed particles secreted by all cells and naturally encapsulate proteins and nucleic acids during biogenesis. EVs mediate intercellular communication, delivering their contents to recipient cells to

[1]Department of Chemical and Biological Engineering, Northwestern University, Evanston, IL, USA. [2]Center for Synthetic Biology, Northwestern University, Evanston, IL, USA. [3]Department of Medicine, Division of Infectious Diseases, Northwestern University Feinberg School of Medicine, Chicago, IL, USA. [4]Center for Pathogen Genomics and Microbial Evolution, Northwestern University Havey Institute for Global Health, Chicago, IL, USA. [5]Interdisciplinary Biological Sciences Training Program, Northwestern University, Evanston, IL, USA. [6]Chemistry of Life Processes Institute, Northwestern University, Evanston, IL, USA. [7]Member, Robert H. Lurie Comprehensive Cancer Center, Northwestern University, Evanston, IL, USA. e-mail: j-leonard@northwestern.edu

affect cellular function[15,16]. Intrinsic properties such as non-toxicity and non-immunogenicity[17,18], as well as the ability to engineer surface and luminal cargo loading, make EVs an attractive vehicle for delivering a wide range of therapeutics. Cargo can be incorporated into vesicles either by overexpressing the cargo in the producer cells such that it is loaded during EV biogenesis or by physically or chemically modifying vesicles post collection[17,19]. Cells that are genetically engineered to produce functionalized EVs may even be implanted to continuously generate such particles in situ[20]. While modification of EVs post collection may confer cargo loading flexibility, this approach requires more extensive purification and introduces challenges from a manufacturing and regulatory standpoint.

Several recent studies have investigated the use of EVs to deliver Cas9 for treatment of cancer, hepatitis B and genetic diseases, highlighting the promise of this method for achieving intracellular Cas9 delivery[21–23]. However, many exploratory studies have used EV engineering methods known to introduce artefacts in downstream experiments, which obscures how functional effects may be attributable to EVs. Of particular concern are methods that rely on transfecting EV producer cells with lipoplexes, loading EVs with electroporation methods known to result in cargo aggregation or isolating EVs with commercial kits not intended for functional delivery applications, which have all been shown to introduce artefacts[24–26].

In this Article, we address this need by developing an integrated bioengineering strategy for genetically engineering cells to direct the self-assembly and production of multifunctional EVs. As a motivating application, we systematically evaluate, compare and generate techniques that enable EV targeting, active loading of protein cargo into EVs, and EV fusion to achieve functional delivery of protein cargo to T cells. This exploration identifies key limitations and drivers of functional EV-mediated delivery, including a potential mechanism of receptor-binding-mediated delivery enhancement to T cells. We validate these technologies by demonstrating a therapeutically relevant capability—the delivery of Cas9 ribonucleoprotein complex (RNP) to ablate the gene encoding the human immunodeficiency virus (HIV) co-receptor CXCR4[27,28] in primary human $CD4^+$ T cells.

Results

Strategy for engineering multifunctional EVs for achieving delivery to T cells

Our overall approach for developing technologies toward the goal of enabling targeted delivery of biomolecules to T cells is to address each limiting step in the process (Fig. 1)—cargo loading into EVs during biogenesis, binding of EVs to specific target-cell receptors, uptake and fusion of the EV with a recipient cell to release cargo into the cytoplasm. Our approach relies entirely upon genetically encodable functions, and we term this strategy GEMINI—genetically encoded multifunctional integrated nanovesicles.

Engineered membrane scaffolds display single-chain variable fragments on EVs

We first investigated strategies for conferring EV targeting. Displaying targeting moieties on the EV surface is one method to promote specific interactions between EVs and target cells and facilitate EV uptake. This strategy was pioneered using display of small peptides[17,19], although we and others have demonstrated that these effects are modest and variable[29]. Recently, display of high-affinity targeting domains, including nanobodies and antibody single-chain variable fragments (scFvs), conferred EV targeting to receptors such as epidermal growth factor receptor (EGFR) and human epidermal growth factor receptor 2[30–32]. We investigated whether this approach could mediate EV targeting to T cells using an anti-CD2 (cluster of differentiation 2) scFv[33]. We selected CD2 as ligand engagement triggers internalization[34], and we hypothesized that such a mechanism could enhance EV uptake upon receptor docking. This could be of particular utility for conferring delivery to T cells, which show low rates of endocytosis and for which delivery of other vehicles is generally challenging[14]. We also chose to avoid targets such as CD3 which could induce non-specific T-cell activation. We selected a distinct display system based on the platelet-derived growth factor receptor (PDGFR) transmembrane domain[19,29]; we hypothesized that using this general strategy may confer display of targeting domains on multiple EV populations, whereas fusion with canonical EV markers (for example, tetraspanins) may bias loading into specific EV subsets. As extravesicular linker design may impact scFv trafficking, folding and target binding, we investigated three candidates: an α-helix to provide structure[33], a 40-residue glycine–serine sequence to provide flexibility or the hinge region of immunoglobulin G4 (IgG4) used in chimeric antigen receptors to display scFvs on synthetic receptors[35]. All three constructs were expressed at comparable levels in human embryonic kidney (HEK293FT) cells (Supplementary Fig. 1a,b), a producer cell line chosen for its high rate of EV production, amenability to biomanufacturing in general (for example, lentivirus production) and to maximize reproducibility across samples in this study (that is, to avoid heterogeneity associated with primary cells and donor-to-donor variability). To test display on EVs, two vesicle populations were isolated using a previously validated differential centrifugation method[36,37]. EVs are best defined by the separation method used for their isolation[26]; for convenience, hereafter the fraction isolated at 15,000 × *g* is termed 'microvesicles' (MVs), and the fraction isolated at 120,416 × *g* is termed 'exosomes'. Vesicles were enriched in canonical markers such as CD9, CD81 and Alix and depleted in the endoplasmic reticulum protein calnexin (Supplementary Fig. 2a). Both populations comprised vesicles averaging ~120–140 nm in diameter and showed the expected 'cup shaped' morphology (Supplementary Fig. 2b,c). Importantly, all three scFv display constructs were substantially expressed in both vesicle populations (Supplementary Fig. 1c).

Display of anti-CD2 scFvs enhances EV binding to Jurkat T cells

To evaluate targeting, we collected vesicles from HEK293FT producer cells stably expressing our scFv constructs and a co-loaded cytosolic dimeric tomato (dTomato) fluorescent protein to evaluate EV binding to and internalization by recipient cells in a manner that avoids artefacts associated with dye-labelling (such as insufficient dye removal or quenching)[38,39]. To facilitate direct comparisons between vesicle subsets, we normalized EV doses by particle count as measured by nanoparticle tracking analysis. EVs were incubated with Jurkat T cells, which express high levels of CD2 (Supplementary Fig. 3), for 2 h—a time point chosen to allow T-cell–EV contact and binding but limit the signal that might be attributed to uptake and accumulation[40]—and then cells were washed to remove unbound vesicles (Supplementary Fig. 4) and analysed by flow cytometry. All three constructs enhanced both MV and exosome binding to T cells (Fig. 2a–c). Display of scFvs on MVs enhanced delivery of dTomato to T cells more so than did display on exosomes, although some—but not all—of this effect is attributable to greater dTomato incorporation in MVs versus exosomes (Supplementary Fig. 5a,b). This differential dTomato loading was not solely attributable to size; exosome volume was ~80% of that of MVs (Supplementary Fig. 2b), and dTomato loading in exosomes was much less than 80% of the loading in MVs. As the helical linker consistently conferred the greatest targeting effect, this design was carried forward for subsequent work.

CD2–scFv binding mediates uptake by recipient cells

We next evaluated whether CD2 engagement by EVs triggers internalization (as noted, ligand binding naturally triggers CD2 internalization[34]). To distinguish EV binding from uptake, cells were treated with trypsin after incubation with EVs to remove non-internalized vesicles, as washing alone did not remove surface-bound particles (Supplementary Fig. 4). Cells receiving targeted vesicles displayed a modest increase in fluorescence over the non-targeted control (Fig. 2d), indicating that

https://doi.org/10.1038/s41551-023-01142-x

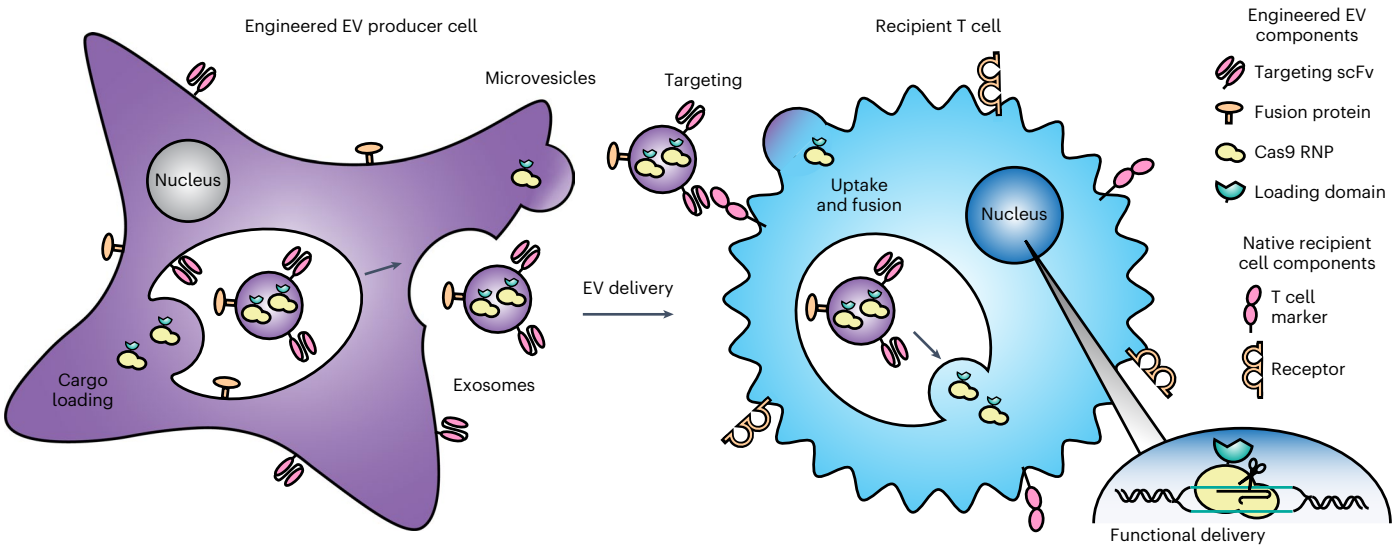

Fig. 1 | Overview of the GEMINI strategy for genetically engineering multifunctional EVs. EV cargo proteins are expressed in producer cells to facilitate incorporation into multiple vesicle populations: MVs, which bud from the cell surface, or exosomes, which are produced by endosomal invaginations into multivesicular bodies. Surface-displayed targeting and fusion proteins aid in binding to and uptake by recipient cells and subsequent cargo release via cell surface fusion or endosomal escape. In the proof-of-principle application explored in this study, the objective is to deliver a Cas9–sgRNA complex to T cells to knock out a gene, as described in subsequent sections.

CD2 targeting can enhance EV uptake. This assay evaluates EV uptake, but it does not directly evaluate EV–recipient-cell fusion or functional cargo release. Therefore, we expect that much of the dTomato signal measured in this way represents EVs in endosomes that may eventually be degraded. Later in this study, we evaluate cargo release into the cytoplasm, which more definitively requires EV–recipient-cell fusion (that is, at the plasma membrane or within an endosome).

CD2–scFv-mediated EV targeting is receptor-specific

To determine whether the observed vesicle and T-cell interactions resulted from specific receptor binding, we pre-incubated recipient Jurkat cells with an antibody binding the same $T11_1$ epitope on CD2 as does our scFv to block potential binding sites. This experimental design enables a direct evaluation of the requirement for specific target engagement without introducing common artefacts associated with differential EV uptake rates when making comparisons across cell types or cell lines[29]. Antibody pre-treatment ablated scFv-enhanced EV binding (Fig. 2e), showing that our targeting is specific for CD2. By contrast, pre-incubation with non-targeted EVs (a potential non-specific competitor) did not substantially reduce either background or scFv-enhanced binding (Supplementary Fig. 6). Together, these data indicate that the scFv mediates specific binding of EVs to CD2.

Optimization of scFv expression increases targeting

Increasing the avidity of interactions between binders (for example, targeted therapeutics) and their receptors is a generally useful strategy for enhancing delivery and function in vivo[41]. To potentially capitalize upon this mechanism, we sought to increase the expression of our scFv constructs and therefore loading into vesicles through mass action. By optimizing the coding sequence of our scFv display construct for expression in human cells using a sliding window algorithm[42], we enhanced cellular expression of our scFv (Supplementary Fig. 7a,b) and increased scFv loading onto vesicles without affecting vesicle size or morphology (Supplementary Fig. 7c–e). EVs generated from cells stably expressing optimized scFv constructs showed enhanced receptor-specific binding to target cells (Fig. 2f). At the end of this limited optimization, targeted EV binding to $CD2^+$ Jurkat T cells exceeded a 100-fold increase over non-targeted EVs. Interestingly, the benefit of codon optimization was more pronounced in MVs than in exosomes, as seen by both scFv incorporation into EVs (Supplementary Fig. 7c) and EV binding to target cells (Fig. 2f), suggesting that increased scFv display confers improved binding. This optimized targeting system also conferred enhanced EV binding and modest EV internalization in primary human $CD4^+$ T cells (Fig. 2g,h), which express high levels of CD2 (Supplementary Fig. 8) and was carried forward for the rest of this study.

CD2–scFv display scaffold influences loading and receptor specificity

Previous reports have achieved scFv display on EVs by fusion to the C1C2 lactadherin domain, which binds to phosphatidylserine on the outer membrane leaflet of some vesicles[30,31,43]. To compare our PDGFR-based display strategy to other state-of-the-art EV scFv display systems, we fused our optimized anti-CD2 scFv to the C1C2 lactadherin domain scaffold (Extended Data Fig. 1a)[30,31,43]. We observed similar expression of both constructs in cells but higher loading of C1C2 scFv constructs (compared to PDGFR constructs) into vesicles (Extended Data Fig. 1b,c). Both systems conferred similar MV binding to Jurkat cells (Extended Data Fig. 1d). C1C2 display appeared to confer some enhancement in exosome binding to T cells (compared to PDGFR display), but C1C2 display targeting was uneven, with only a subset of Jurkat recipient cells bound strongly to C1C2 display EVs, whereas PDGFR display targeting generally mediates delivery to the entire population of T cells (Extended Data Fig. 1e). As this pattern might provide evidence of CD2-independent EV binding (which would comprise an artefact), we investigated whether C1C2 display targeting was CD2 specific. Pre-incubation of EVs with an anti-CD2 antibody mediated only a partial reduction in C1C2 display targeted EV binding (in contrast to PDGFR display targeting), suggesting the existence of substantial non-target-specific mechanisms for C1C2 display targeting of EVs using this scFv (Extended Data Fig. 1f,g). Given these observations, we opted to proceed with the validated and efficient PDGFR display of scFvs to achieve EV targeting.

Abscisic-acid-inducible dimerization domains enable an active EV cargo loading system

We next sought to engineer our scFv-containing EVs to load a therapeutic cargo of interest. Overexpression of cytosolic cargo in EV producer cells results in passive loading into vesicles during biogenesis via mass

https://doi.org/10.1038/s41551-023-01142-x

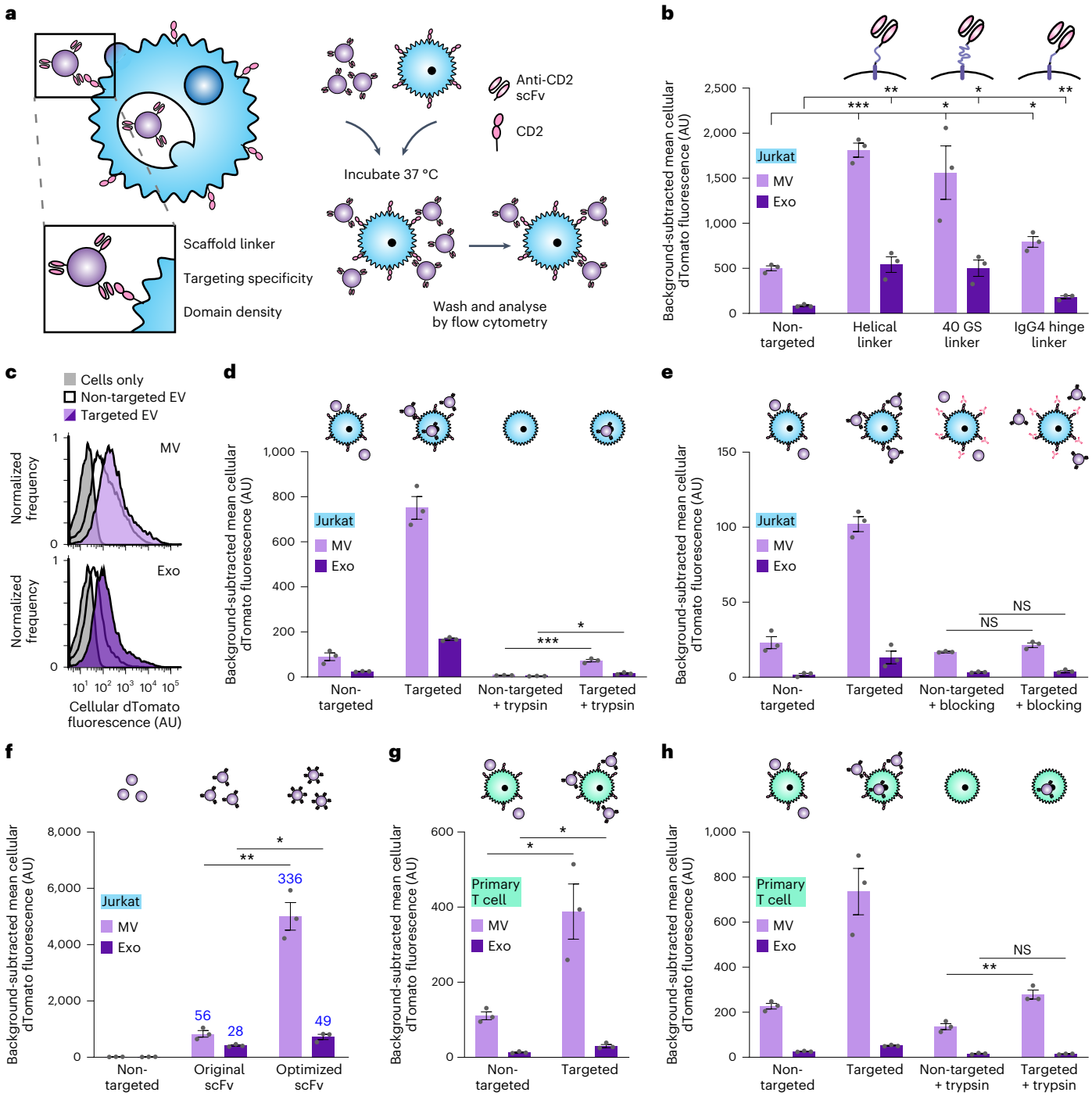

Fig. 2 | Display of scFvs on EVs mediates receptor-specific, targeted binding and uptake to T cells. a, Strategy for targeting EVs to T cells (left) and illustration of EV binding experiments (right). **b**, Targeted EVs binding to Jurkats (2 h incubation). To evaluate potential differences in dTomato loading, average EV fluorescence was analysed separately (Supplementary Fig. 5). Exo, exosome; 40 GS, 40-residue glycine–serine. **c**, Representative histograms depicting distributions of helical linker EV-mediated fluorescence in recipient cells analysed in **b**. **d**, Distinguishing binding and internalization for EVs targeted to Jurkats. Trypsinization was used to remove bound, non-internalized EVs following a 6 h incubation. **e**, Specificity of EV targeting to CD2. Pre-incubation with anti-CD2 antibodies ablated EV targeting to Jurkats. NS, not significant. **f**, Enhancement of targeting by codon-optimized expression of scFv constructs. Fold increases over the non-targeted control are reported in blue. **g**, Binding of targeted EVs to primary human $CD4^+$ T cells (2 h incubation). **h**, Distinguishing binding and internalization for EVs targeted to primary human $CD4^+$ T cells. All experiments were performed in biological triplicate, and error bars indicate standard error of the mean. Statistical tests comprise two-tailed Student's *t*-tests using the Benjamini–Hochberg method to reduce the false discovery rate. $^*P < 0.05$; $^{**}P < 0.01$; $^{***}P < 0.001$. Exact *P* values are reported in Supplementary Table 1. EV dTomato loading evaluations are in Supplementary Fig. 5.

action[40]. Increasing cargo content in EVs would potentially produce a more potent delivery vehicle. To both enhance cargo protein loading and increase the likelihood that a given vesicle will incorporate both a cytosolic cargo protein and our membrane-bound scFv, we designed a small molecule dimerization-based loading system (Fig. 3a). Systems using light or small molecules (for example, rapamycin) as inducers have been reported to aid EV cargo loading[44,45], but light is difficult to scale to large volumes and rapamycin-induced dimerization is so

https://doi.org/10.1038/s41551-023-01142-x

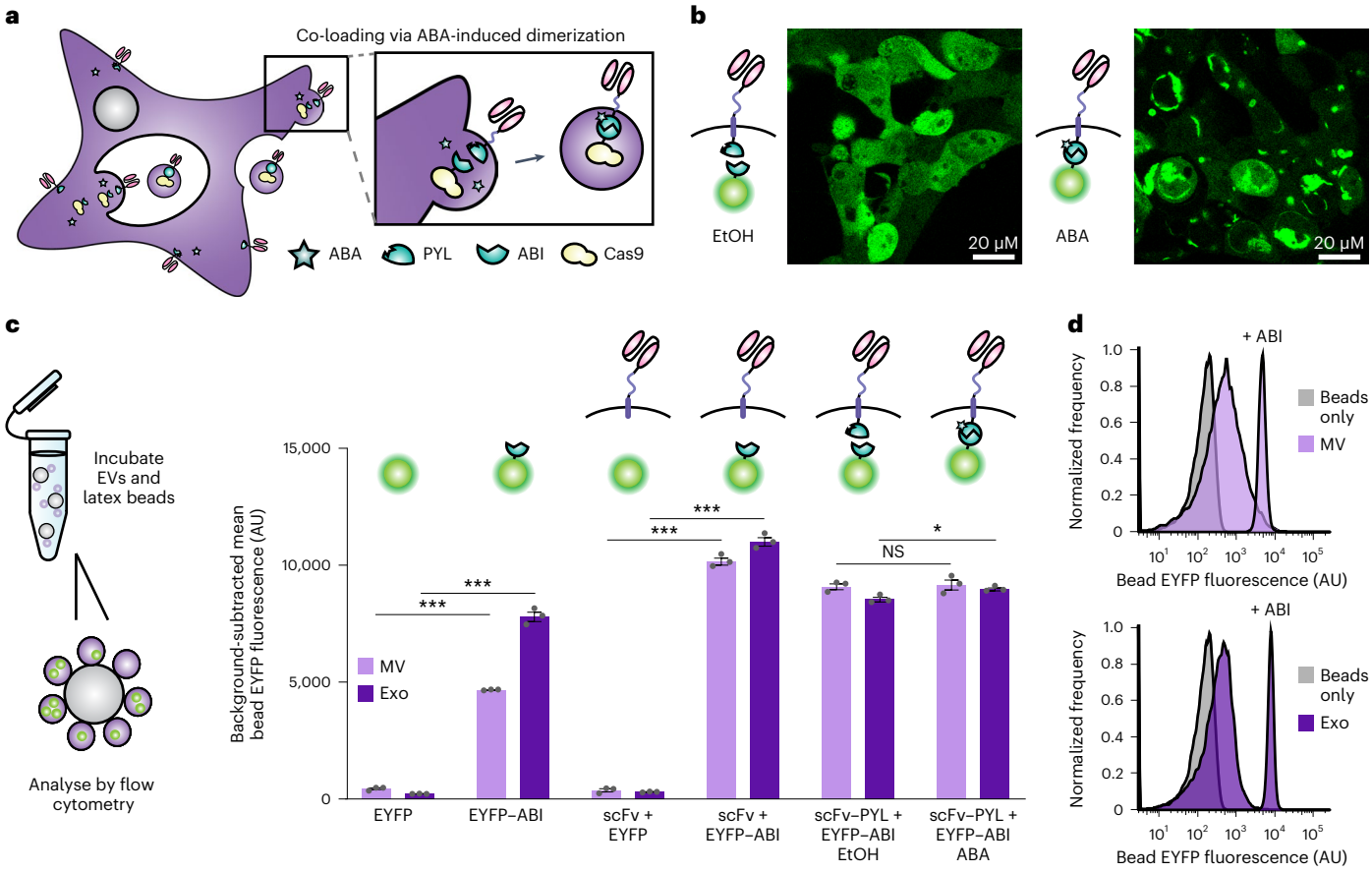

Fig. 3 | Cargo protein is actively loaded into EVs via tagging with the ABI domain of the ABA dimerization system. a, Illustration of ABA-based dimerization of EV cargo proteins and subsequent loading into vesicles. **b**, ABA-induced dimerization between PYL and ABI domains. Illustrative microscopy showing anti-CD2 scFv–PYL (membrane bound) and EYFP–ABI (cytosolic) association in the presence of ABA. Full images are in Supplementary Fig. 10. **c**, ABI-induced cargo loading into EVs. EVs generated under conditions indicated were adsorbed to aldehyde/sulfate latex beads and analysed by flow cytometry to determine bulk average fluorescence. Experiments were performed in biological triplicate, and error bars indicate standard error of the mean. Statistical tests comprise two-tailed Student's *t*-tests using the Benjamini–Hochberg method to reduce the false discovery rate. $^{*}P < 0.05$; $^{**}P < 0.01$; $^{***}P < 0.001$. Exact *P* values are reported in Supplementary Table 1. **d**, Representative histograms of EYFP ± ABI conditions in **c** (two leftmost sets of bars). **e**, Active loading of Cas9–ABI with and without an NLS into EVs. About 6.0×10^8 EVs were loaded per lane. Expected band sizes (~160 or 195 kDa, arrows) correspond to Cas9 ± the ABI domain. The full blot is provided in Extended Data Fig. 3d. **f**, Analysis of ABA-dependent Cas9–ABI loading into EVs enriched for anti-CD2 scFv–PYL via affinity chromatography. About 1.3×10^7 MVs or 2.0×10^7 exos were loaded per lane. Expected band size = 195 kDa (arrows). Full blots are provided in Supplementary Fig. 11b. **g**, Bioactivity of EV-associated Cas9. Vesicles were lysed and incubated with a linearized target plasmid for 1 h at 37 °C in Cas9 nuclease reaction buffer. Expected cut band sizes = 7.6 and 4.6 kb (arrows). For all gels, cropped regions are annotated in the Source Data.

tight that it is functionally irreversible[46]. Therefore, we explored a new strategy based on the plant hormone abscisic acid (ABA)-inducible interaction between truncated versions of the abscisic acid insensitive 1 (ABI) and pyrabactin resistance-like (PYL) proteins[47]. This 'ABA' system confers several advantages: association is rapid; the dimerization is reversible, presumably allowing for cargo release in recipient cells; ABA is inexpensive and non-toxic; and small-molecule-regulated loading is more readily applicable to biomanufacturing than is control by light. We first investigated fusing the ABI and PYL domains to the luminal side of our scFv construct and to either the 5′ or 3′ end of a cytosolic or nuclear-localized enhanced yellow fluorescent protein (EYFP) cargo protein to determine effects on protein expression and function. Fusion with the PYL domain reduced expression (or destabilized) EYFP (Supplementary Fig. 9a), while the scFv was tolerant to fusions with either ABI or PYL domains (Supplementary Fig. 9b,c). Thus, we moved forward with the scFv–PYL and EYFP–ABI (3′ fusion) constructs. ABA-induced dimerization of ABI and PYL in this set-up was readily evident in fluorescence distribution changes upon ligand addition observed by microscopy (Fig. 3b and Supplementary Fig. 10).

The ABI domain alone drives protein incorporation into EVs

To investigate cargo protein loading, vesicles were adsorbed to latex beads and analysed by flow cytometry. No increase in EV loading was observed with ABA treatment, and across all conditions, constructs containing the ABI domain showed a higher degree of loading than did those lacking this domain (Fig. 3c,d). This effect was not attributable to ABI-dependent increases of protein expression in producer cells (Extended Data Fig. 2a). ABI-enhanced loading was evident when paired with the scFv alone or the scFv–PYL construct, indicating that intrinsic ABI-enhanced loading is independent of ABI–PYL interactions (Fig. 3c). The presence of the scFv conferred an added benefit in protein loading over an EYFP–ABI-only control (Extended Data Fig. 2b). Although no known mechanism explains this result, one possibility is that alterations in the local lipid environment caused by the scFv loading may favour the mechanism by which ABI confers loading of cargo proteins into EVs. To investigate the role of subcellular localization on the EV loading process, we introduced a nuclear localization sequence (NLS) to EYFP–ABI and compared loading to the purely cytosolic construct. ABA-induced dimerization again had a negligible effect on cargo loading, and addition of an NLS to EYFP–ABI did not diminish loading into EVs (Extended Data Fig. 2c). Altogether, these data support the serendipitous discovery that ABI comprises a potent EV cargo protein loading tag.

The ABI domain mediates Cas9 loading into EVs

We next investigated whether ABI can be used to load EVs with functional cargo. For this, we selected *Streptococcus pyogenes* Cas9, as Cas9 can be synthesized in producer cells (and is thus consistent with the GEMINI strategy) and because Cas9 must travel to the nucleus of recipient cells to act on genomic targets. ABI was fused to the N- or C-terminus of Cas9, and, in general, expression patterns matched those observed for EYFP with improved expression of C-terminally tagged Cas9 (Extended Data Fig. 3a). Thus, we moved forward with the Cas9–ABI (3′ fusion) constructs. We also investigated whether addition of an NLS or ABI domain impacted Cas9 loading and function; although addition of multiple NLS sequences can increase Cas9 efficacy[48], nuclear localization could also inhibit loading of Cas9 into EVs. Thus, we chose to investigate the addition of a single N-terminal NLS fusion to balance these effects. When expressed via transfection (along with a cognate sgRNA targeting a reporter construct) in reporter Jurkat T cells—a system similar to the stoplight reporter developed by de Jong et al.[49], Cas9 fusion constructs showed similar nuclease activity to Cas9 alone (Extended Data Fig. 3b,c). When Cas9 constructs were expressed in EV producer cells, the NLS minimally influenced Cas9 loading into EVs, while the ABI domain noticeably increased Cas9 loading (Fig. 3e and Extended Data Fig. 3d) but not overall expression in producer cells (Extended Data Fig. 3e). These trends are consistent with those observed with EYFP and show the utility of the ABI loading tag across multiple cargo proteins.

Membrane scFvs and ABI-fused Cas9 co-load into EVs

An important, but largely unexplored, factor to consider in engineering EV-based therapeutics is the extent to which multiple cargo types localize to the same vesicles in a population. Although ABI alone loads protein into EVs, it remained unknown whether dimerization of cargo and display proteins could enhance co-loading into EVs (that is, co-loading of both the scFv and Cas9 into individual vesicles). To evaluate this question, we generated vesicles from cells expressing scFv–PYL and Cas9–ABI treated with ABA or a vehicle control and isolated anti-CD2 scFv-displaying vesicles via the 3× FLAG tag located on the N-terminus of the scFvs by affinity chromatography (Supplementary Fig. 11a)[50]. High levels of Cas9 were found in scFv-enriched vesicles, independent of ABA treatment, indicating that ABI-tagging of cargo is sufficient to achieve substantial scFv and Cas9 co-loading in EVs (Fig. 3f and Supplementary Fig. 11b). Formally, these data indicate that Cas9 is associated with EVs that express the scFv on the surface; they do not determine whether Cas9 is in the EV lumen, on the EV surface or both.

EV-loaded Cas9 shows nuclease function

To evaluate whether EV-encapsulated Cas9 RNPs are functional, we devised a direct in vitro assay. EVs from Cas9 and sgRNA-expressing cells were lysed and incubated with a plasmid encoding the sgRNA target sequence (Fig. 3g). Plasmids treated with lysed RNP-containing EVs showed the expected specific cleavage products under all conditions tested. The presence or absence of an NLS did not impact cleavage efficiency in this assay, but Cas9 fused to the ABI domain showed some reduced cleavage for both vesicle populations. As it is not clear whether this partial effect (for example, a potential reduction in Cas9 turnover rate) is meaningful in a cellular delivery context (further consideration in 'Discussion'), both ABI+ and ABI− constructs were evaluated in subsequent experiments.

Viral glycoprotein display increases EV uptake by T cells

To promote EV uptake and fusion, we investigated displaying viral glycoproteins on EVs. We first investigated vesicular stomatitis glycoprotein (VSV-G), which is commonly used in lentiviral pseudotyping and has been reported to confer EV fusion with recipient cells[51,52]. VSV-G was transiently expressed in dTomato-expressing producer cells, and the resulting EVs were incubated with recipient T cells for 16 h (this time point was chosen to allow time for EV binding, internalization and potential accumulation of EVs in intracellular compartments) before trypsinization (to remove non-internalized vesicles) and analysis by flow cytometry. VSV-G enhanced EV uptake in both Jurkat T cells (Fig. 4a,b) and primary human $CD4^+$ T cells (Fig. 4c), establishing the utility of viral fusion proteins for delivering EVs to T cells.

To develop a system that confers EV binding, uptake and/or fusion in a manner that is more targeted to T cells (as VSV-G mediates fusion to most cell types)[53], we investigated the use of truncated versions of the measles virus glycoproteins haemagglutinin (H) and fusion (F), which have previously been used to aid lentiviral delivery to T cells[54,55]. These proteins bind signalling lymphocyte activation molecule F1 (SLAM) and/or the complement regulator CD46, both of which are expressed on diverse T cells[56]. H/F proteins are classically believed to mediate viral fusion at the cell surface[57], although it has also been reported that viral endocytosis can be mediated by SLAM[55,58]. In the same fluorescent EV uptake assay described above, we investigated EV delivery to Jurkats (which minimally express SLAM), SLAM-transgenic Jurkats or primary human T cells that express SLAM (Fig. 4d). H/F proteins conferred

https://doi.org/10.1038/s41551-023-01142-x

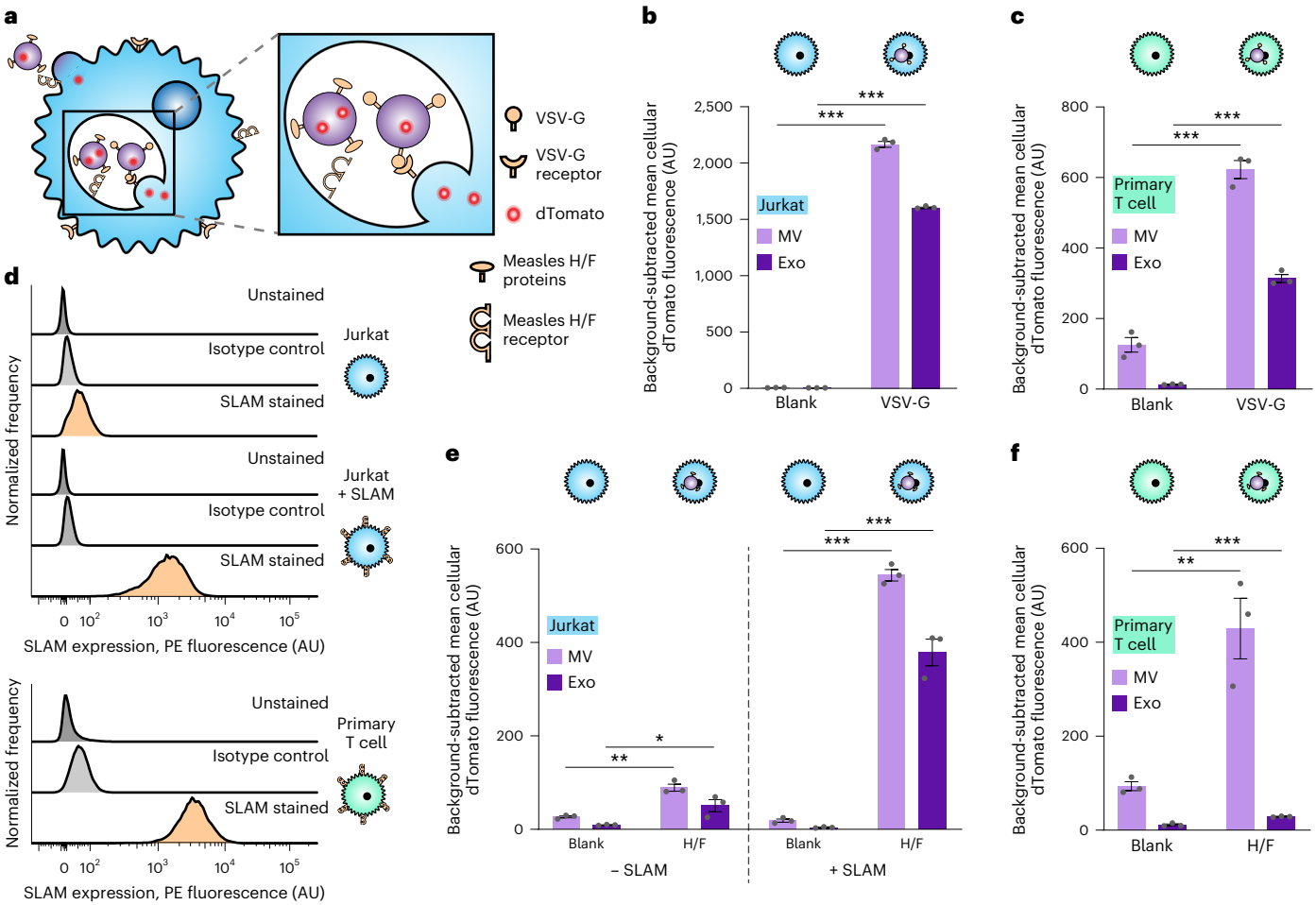

Fig. 4 | Viral glycoprotein display on EVs mediates uptake by recipient T cells. a, Illustration of viral glycoproteins facilitating EV uptake and fusion at either the plasma membrane or in the endosome. **b**, Uptake of dTomato-labelled VSV-G EVs by Jurkat T cells. **c**, Uptake of dTomato-labelled VSV-G EVs by primary human CD4$^+$ T cells. **d**, Surface expression of SLAM on T cells. Unmodified Jurkats, Jurkats expressing transgenic SLAM, or primary human CD4$^+$ T cells were evaluated for SLAM surface expression by flow cytometry. **e**, Uptake of dTomato-labelled measles viral glycoproteins H/F EVs by Jurkats (±SLAM). **f**, Uptake of dTomato-labelled measles virus glycoproteins H/F EVs by primary human CD4$^+$ T cells. In all cases, EVs were incubated with cells for 16 h and trypsinized to remove surface-bound vesicles. Experiments were performed in biological triplicate, and error bars indicate standard error of the mean. Statistical tests comprise two-tailed Student's *t*-tests using the Benjamini–Hochberg method to reduce the false discovery rate. $^*P < 0.05$; $^{**}P < 0.01$; $^{***}P < 0.001$. Exact *P* values are shown in Supplementary Table 1. EV dTomato loading evaluations are in Supplementary Fig. 12.

modest EV uptake to parental Jurkats (SLAM$^-$), but these proteins substantially enhanced EV uptake by SLAM-transgenic Jurkats and primary human CD4$^+$ T cells (Fig. 4e,f). We also explored an alternative, non-viral protein-based strategy reported to promote functional transfer by overexpressing constitutively active connexin 43 (Cx43), a protein involved in the formation of gap junctions, on EV producer cells[20,59]; Cx43-mediated delivery by EVs had not yet been evaluated in the context of delivery to T cells. Cx43 did not confer increased EV internalization by T cells in this application, so this approach was not further investigated (Supplementary Fig. 13). Altogether, these results support the use of the measles H/F glycoproteins as a method for enhancing EV uptake by SLAM$^+$ T cells.

EVs mediate functional delivery of Cas9 to primary T cells

Evaluating functional delivery of Cas9 to recipient T cells requires effective cargo loading, T-cell binding and fusion, and subsequent release of active Cas9 RNPs, and having validated each of these steps individually, we proceeded to evaluate the combined technologies—the first combined test of the GEMINI strategy. Specifically, we investigated the use of Cas9 to target the CXCR4 locus in primary T cells using a previously validated sgRNA; CXCR4 is a clinically relevant target for the treatment of HIV[60–62]. We validated this sgRNA and confirmed that it is required for Cas9-mediated CXCR4 target cleavage (Supplementary Fig. 14). As viral glycoprotein expression is cytotoxic, at this point we pivoted to biomanufacturing EVs using a Lenti-X HEK293T cell line that is well suited to this challenge; this line was selected for its ability to produce high lentiviral titres. EVs containing the anti-CD2 scFv, NLS Cas9–ABI with the appropriate sgRNA, and either VSV-G or measles virus glycoproteins H/F were incubated with primary human CD4$^+$ T cells for 6 days before collecting genomic DNA. This time point was chosen to allow sufficient time for EV binding, internalization, fusion, endosomal escape, Cas9 release, nuclear trafficking, cleavage and double-strand-break repair. Samples were analysed via high-throughput sequencing (HTS), providing a sensitive and unambiguous readout of functional delivery. Editing events were quantified and characterized in a region of 64 nucleotides centred around the expected cleavage site. Excitingly, indels were identified at the predicted Cas9 cut site for all vesicle treatments containing Cas9 RNPs (Fig. 5 and Supplementary Fig. 15). VSV-G display on EVs conferred higher editing efficiencies than measles H/F proteins did, and exosome treatments conferred more edits than MV treatments did for matched designs. The majority of edits were classified as deletions with a smaller number of insertion events or edits consisting of both an

https://doi.org/10.1038/s41551-023-01142-x

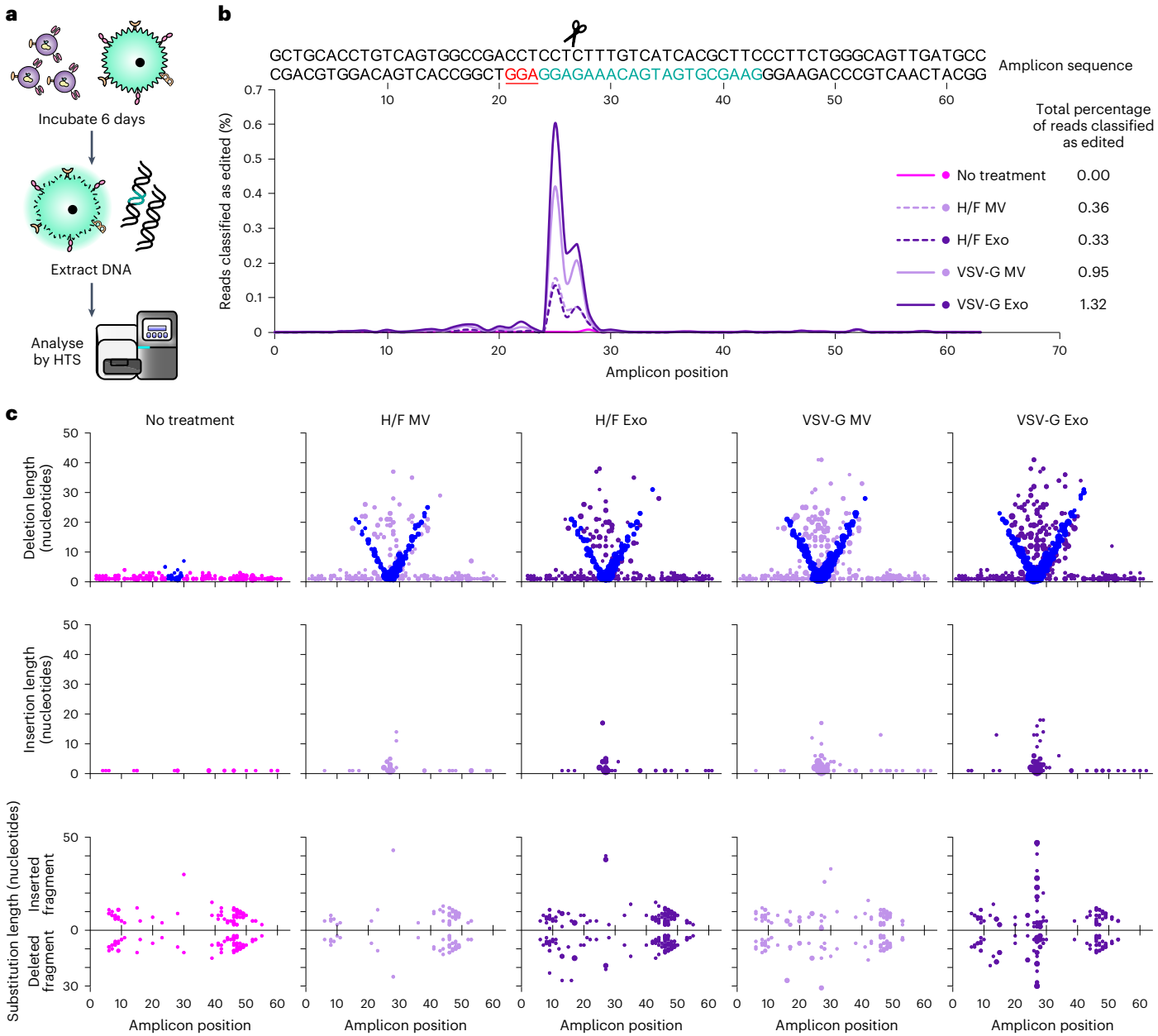

Fig. 5 | EVs mediate functional delivery of Cas9 in primary human T cells. **a**, Illustration of function delivery evaluation. About 2.0×10^{10} EVs were incubated with 5.0×10^{4} $CD4^{+}$ T cells for 6 days before genomic DNA extraction and HTS analysis. **b**, Frequency of indels detected at the Cas9-targeted CXCR4 locus. The sgRNA recognition site (green), protospacer adjacent motif (PAM) sequence (underlined, red) and predicted cut site (amplicon position 26, scissors) are shown. Total percentage of HTS reads classified as 'edited' represents the area under the histogram trace shown for each sample. **c**, Distributions of EV–Cas9-mediated edits, by type. DNA amplicon position is plotted on the abscissa and length of the edit observed is plotted on the ordinate, while the size of each dot scales with the number of edits that meet that description. Each read is uniquely classified as a deletion, insertion or substitution such that no one read contributes to more than one dot in this panel. In the case of substitutions, the positive ordinate reports the insertion portion of the edit, and the negative ordinate reports the deletion portion of the edit such that each edit is represented by two dots. In this panel, deletions are reported by placing a dot at the midpoint of the deleted segment. To help explain the apparent 'V' pattern, dots are coloured blue to indicate cases where one end of the deleted segment corresponds to the predicted cut region, presumably corresponding to a subset of the DNA repair outcomes observed. Sample dot colouring is as in **b**.

insertion and a deletion. This overall pattern is consistent with previous reports of Cas9 RNP editing at this locus[60] in that edits comprise mostly small deletions and insertions centred around the cleavage locus, indicating that EV-mediated delivery of Cas9 using GEMINI yields effects that are qualitatively comparable to electroporation of recombinant Cas9 RNPs. Although systematic evaluation of EV cytotoxicity has been reported[63] and systematic re-evaluation of these new EV formulations is beyond the scope of the current study, we generally did not observe any overt impairment (for example, reduced T-cell proliferation or altered scattering in flow cytometry) in samples treated with engineered vesicles. To evaluate the role of ABI-mediated active loading in functional delivery, we generated EVs with Cas9 ± ABI and evaluated editing efficiencies in primary T cells. The two Cas9 variants performed comparably well in this context, despite previously noted trade-offs in loading and specific cleavage activity (Supplementary Fig. 16).

To further explore the mechanism of EV-mediated Cas9 delivery to T cells, we investigated delivery of NLS Cas9–ABI EVs displaying the anti-CD2 scFv and VSV-G to the reporter Jurkat line described in

Extended Data Fig. 3. Treatment with Cas9 EVs produced a small yet significant degree of fluorescent reporter conversion (Supplementary Fig. 17). As production of the fluorescent reporter from the stably integrated reporter locus can only occur after Cas9 cleavage and appropriate non-homologous end joining correction, this provides unambiguous evidence of EV-mediated delivery of functional Cas9 RNPs.

To benchmark EV-mediated Cas9 delivery to a state-of-the art method used in vitro, we evaluated Cas9 RNP electroporation as a point of comparison. Although the methods of delivery differ substantially, we decided to compare ultimate gene editing rates on the basis of Cas9 dose per cell. We first quantified Cas9 molecules per EV via western blot using a purified Cas9 calibration curve, from which we estimated a loading of ~100 Cas9–ABI molecules per EV (Extended Data Fig. 4a,b). We then investigated the rate of CXCR4 editing in primary T cells using a standard, optimized RNP electroporation protocol[64]. For similar doses of Cas9/cell used in EV delivery, we observed CXCR4 editing rates of 15–60% for RNP delivery (Extended Data Fig. 4c). Interestingly, while overall editing patterns were generally similar across delivery methods (in terms of position and relative amounts of deletions and insertions), RNP-mediated edits strongly favour very short deletions compared to other types of edit, and this preference was greater than that observed for EV-mediated delivery (Extended Data Fig. 4d). Although this comparison is somewhat apples-to-oranges, it nonetheless suggests opportunities for future optimization ('Discussion').

Having achieved functional delivery with our multifunctional EVs, this enabled us to next interrogate the specific contributions of each engineered EV feature. In particular, we sought to evaluate the unique contribution of the anti-CD2 scFv, as it can confer some degree of binding and uptake in vitro. To ascertain the requirement of EV scFv–CD2 engagement for functional delivery, we pretreated and cultured cells with an anti-CD2 antibody before EV addition to block receptors on recipient cells. Notably, we found that pretreatment with the anti-CD2 antibody increased editing rates across vesicle types and viral glycoprotein systems (Fig. 6a,b). To explain this observation, we hypothesized that engagement of CD2 might result in higher levels of T-cell activation and make cells more susceptible to EV uptake and editing, as CD2 engagement is known to have T-cell co-stimulatory activity[33]. To investigate this possibility, we incubated T cells with either EV scFvs or anti-CD2 antibodies and analysed surface expression of CD25. As EV uptake (and thus CD2 engagement) was evident within 1 day (Fig. 4), we examined any potential upregulation of CD25 on the following day. CD25 expression was minimally impacted by any treatment, indicating that T-cell activation cannot explain the observed increase in editing upon CD2 engagement (Supplementary Fig. 18). To investigate how editing efficiency scales with practical considerations such as EV dose, and to probe how CD2 engagement may contribute to this process, we evaluated EV delivery to T cells from two distinct donors using only a single EV dose or repeating EV administration every day for the 6 days of incubation (Fig. 6c,d). As expected, repeat EV administration increased editing efficiency in all cases, indicating that redosing is a useful handle for boosting editing. In general, scFv–CD2 engagement enhanced editing mediated by exosomes as compared to no CD2 engagement or engagement by a soluble antibody, and this effect was less pronounced, although still evident, for MV-mediated editing. Finally, to evaluate which trends hold across experiments, we performed a combined analysis (normalizing to control for variables hypothesized to contribute to variation in editing efficiency, such as donor T-cell batch-specific susceptibility to Cas9 RNP-mediated editing[61]) (Fig. 6e,f). While a larger-scale study is necessary to rigorously quantify donor-to-donor variation[65], overall, these combined trends support the key conclusions noted above—VSV-G display outperforms H/F in enabling EV-mediated functional delivery to activated $CD4^+$ T cells; multiple EV doses result in higher degrees of editing; and CD2 engagement enhances the ultimate level of target editing.

Discussion

We developed the GEMINI strategy of combining genetically encoded general approaches for targeting EVs to recipient cells with surface-displayed scFvs, actively loading EVs with protein cargo via tagging with vesicle-localizing domains, and promoting uptake and fusion with recipient cells by displaying viral glycoproteins. The motivating application of achieving Cas9 delivery to T cells—a challenging objective—proved useful for refining and validating technologies that can be combined to achieve this goal.

An exciting aspect of EV-mediated delivery is the potential to target vesicles to cells and receptors of interest through engineered interactions. Previous reports have shown non-targeted EV-mediated transfer to T cells, with cargo including EV-encapsulated AAV8[66] or zinc finger-fused methyltransferases[67]. EVs that bind T cells have also been described as a method of crosslinking T cells and other cellular targets by displaying linked anti-CD3 and anti-EGFR scFvs on the PDGFR transmembrane domain[68]. Here we have shown both EV targeting and EV uptake by T cells. We anticipate that the modularity of our targeting construct will be useful for directing EVs to other cell types and receptors.

One technology reported here involved the serendipitous discovery that the ABI domain (from the ABA dimerization system) facilitates EV cytosolic cargo protein loading even without ABA. The mechanism of this effect is unknown. ABI is not predicted by WoLF PSORT (https://www.genscript.com/wolf-psort.html) to localize to the cell membrane or endosomal pathways. An advantage of this system is that ABI-mediated loading is easier to implement than multi-domain dimerization systems (using light[44], rapamycin[45] or dimerization (Dmr) domains[69]) or tags that require overexpression of helper proteins to facilitate trafficking into vesicles, such as the WW domain and Nedd4 family interacting protein 1 (Ndfip1)[70]. Other active loading tags have recently been explored by Codiak Biosciences[71], in this case deriving a tag from a membrane-associating protein, although the reversibility of such interactions has yet to be established. While the ABI-mediated EV loading strategy may provide advantages over other systems, it will be important to evaluate how this as-of-yet unknown mechanism extends to other cell types. Although increased Cas9 loading did not confer additional DNA cleavage in our in vitro assay, potentially because this particular Cas9 fusion strategy reduced Cas9 turnover rate (Extended Data Fig. 3c), higher cargo loading is likely beneficial in cell delivery contexts where EVs must overcome additional barriers of uptake, fusion, cytosolic release and intracellular trafficking. In such contexts, the advantage of delivering more Cas9–sgRNA cargo may outweigh slower reaction rates. A key consideration that informs the interpretation of editing data is that although each target cell has only two CXCR4 target loci, each locus can be cleaved, correctly repaired, and re-cleaved many times before the ultimate introduction of an error that can be detected by sequencing. If generating an observable edit indeed requires many cleavage events, it is possible that the benefits of Cas9 copy number and activity are balanced in such a way that active loading functional effects are minimal. In the future, it is also possible that the ABI fusion strategy may be refined in future work to mitigate any effects on Cas9 activity.

The eventual fate of EVs in recipient cells is often degradation in the endosomal/lysosomal pathway[40], and thus developing methods to achieve vesicle fusion in recipient cells is critical for achieving (or enhancing) functional cargo delivery (that is, to the cytoplasm). Here we demonstrated the use of VSV-G and measles virus glycoproteins H/F to achieve efficient internalization of EVs by both Jurkat and primary T cells for VSV-G and in cells expressing the lymphocyte receptor SLAM for H/F. A translational consideration is that mutant versions of the H/F proteins have been developed to evade pre-existing neutralizing host antibodies, such as those induced by the measles vaccine[72]. Nonetheless, the use of viral components in general may elicit immune responses (especially in the context of re-administration over time), and a future opportunity is mediating fusion without using exogenous

https://doi.org/10.1038/s41551-023-01142-x

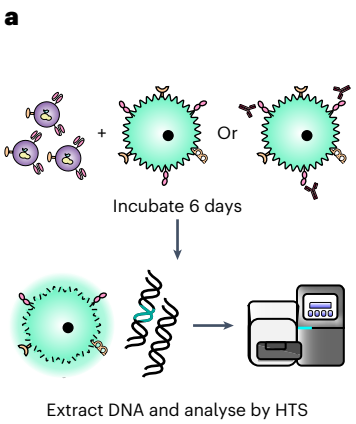

b

Vesicle type	Viral glycoprotein	Targeting	Total percentage edited
No treatment	N/A	N/A	0.00
MV	Measles H/F	Anti-CD2 scFv	0.29
Exo			0.35
MV	VSV-G		1.79
Exo			2.00
MV	Measles H/F	Anti-CD2 scFv + anti-CD2 blocking Ab	0.56
Exo			0.82
MV	VSV-G		2.78
Exo			2.99

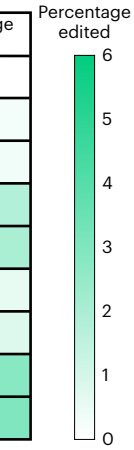

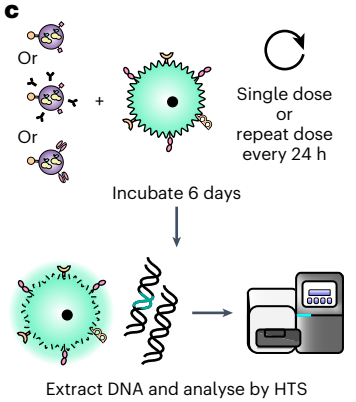

d

		Donor 1 Non-targeted	Donor 1 Non-targeted + soluble Ab	Donor 1 Targeted	Donor 2 Non-targeted	Donor 2 Non-targeted + soluble Ab	Donor 2 Targeted
MV	Single-dose	0.95	0.97	0.69	0.82	1.31	1.15
	Multi-dose	2.76	3.19	2.82	4.23	4.68	5.51
Exo	Single-dose	0.18	0.17	0.24	0.16	0.08	0.76
	Multi-dose	0.56	0.79	1.03	0.87	1.30	3.14

Total percentage edited

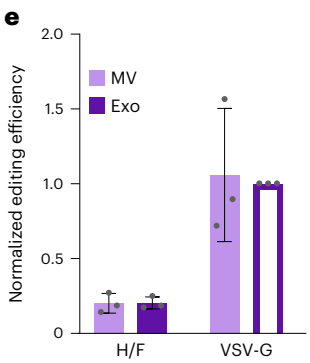

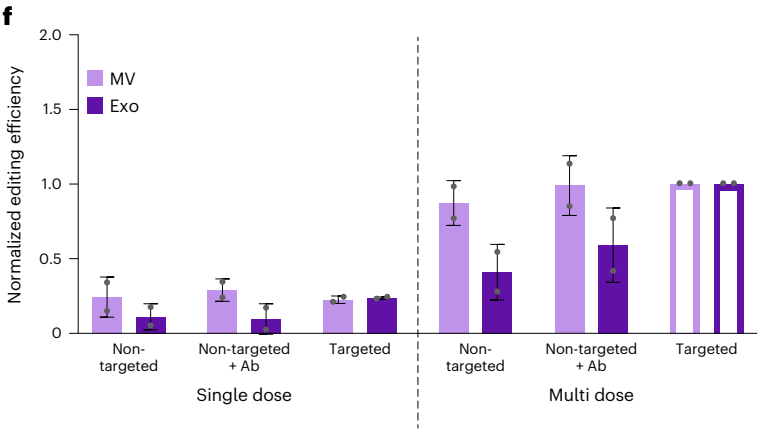

Fig. 6 | CD2 engagement and repeat dosing enhance EV-mediated functional cargo delivery and vary with vesicle subpopulation. a, Illustration of strategy for probing the requirement of scFv–CD2 engagement by blocking CD2. **b**, Blocking CD2 on recipient cells before EV addition increases total editing for all vesicle types. About 8.0×10^9 EVs were incubated per 4.0×10^4 $CD4^+$ T cells for 6 days before genomic DNA extraction and HTS analysis. Heat map colouring scales from 0–6% total Cas9-mediated editing. Ab, antibody. **c,d**, Illustration (**c**) and evaluation (**d**) of experiments probing Cas9-mediated editing after repeat EV administration and various modes of CD2 engagement. Two independent experiments using different donor cells and EV preparations are shown to explicitly capture variation across experiments. EV dosing was as follows: donor 1–1.25×10^{10} MVs or 5.50×10^9 exos per 5×10^4 cells; donor 2–1.50×10^{10} MVs or 7.50×10^9 exos per 5×10^4 cells. Heat map colouring is as in **b**. **e**, EV-mediated Cas9 functional delivery shows consistent trends across three donors and EV batches. Editing efficiency was normalized to the sample receiving VSV-G exosomes (open bar) for each of three independent experiments. **f**, Combined analysis of experiments presented in **d**. Within each vesicle population, editing efficiencies were normalized to the sample receiving multiple doses of VSV-G EVs (open bars); this normalization strategy is designed to control for expected sources of greatest variation (that is, intrinsic donor/T-cell batch-specific susceptibility to EVs and editing). Error bars represent one standard deviation.

viral components, such as has been demonstrated by using endogenous retrovirus-derived syncytin display on virus-like particles[9]. In functional Cas9 delivery studies, we observed greater Cas9 editing efficiencies in activated primary T cells using vesicles functionalized by VSV-G compared to H/F. Both viral protein systems have been used in the analogous process of pseudotyping lentivirus vectors, and previous observations suggest that the H/F proteins may be more suitable for delivery to resting T cells even if they confer no advantage over VSV-G in delivery to activated T cells[54]. A further consideration is that while this study focused on increasing the efficiency of EV-mediated

delivery to T cells, future work is likely needed to evaluate and develop complementary strategies to achieve specific delivery (that is, to avoid delivery to non-target cells that express receptors for the viral glycoproteins used in this study).

Our observed conversion efficiencies, although modest at the doses used in this exploration, meet or exceed comparable reports in the literature, and our analyses indicate interesting opportunities for future work. Perhaps the most rigorous and compelling comparator study reported that 12 repeat, high-dose ($\sim 1 \times 10^{11}$ EVs compared to our $\sim 1 \times 10^{10}$ EVs) administrations of vesicles derived from MDA-MB-231 breast cancer cells loaded with an sgRNA were required to achieve conversion efficiencies on the order of 0.1% in HEK293T reporter cells that constitutively express Cas9 (a cell type to which delivery of viral vectors and various biomolecules is fairly efficient compared to T cells)[49]. We observed substantially greater conversion rates in our system, and conversion increased with repeat administration for both EV types. Although standard RNP electroporation is quite a distinct physical process compared to EV delivery, the greater efficiency observed when electroporating equivalent doses of Cas9 inspire some speculation as to possible avenues for increasing the efficiency of EV-mediated delivery. First, electroporation physically disrupts cell membranes, so increasing the rate of EV–target-cell fusion could help improve that step of delivery. Second, Cas9 RNPs synthesized by EV producer cells contain natural sgRNAs, while recombinant RNPs use chemically modified guide RNAs; chemical modifications of guide RNAs reduce nuclease susceptibility and enhance genome editing[73]. In one study, delivery of plasmids encoding sgRNA and Cas9 to primary T cells resulted in no editing above background, while transfecting a Cas9-expression plasmid along with chemically modified sgRNA led to substantial editing[73]. This limitation thus appears to reflect a feature of Cas9 cargo systems, rather than a general limitation on EV-mediated delivery, but nonetheless is it possible that a similar complementation strategy (for example, transfection of chemically modified sgRNA into EV-producing cells) could enhance EV-mediated delivery of functional Cas9 RNPs. Similarly, we did not quantify the levels of sgRNA found in EVs nor the ratio of sgRNA to Cas9 protein; it is possible that modifying production format could increase the fraction of Cas9 proteins that are present as functional RNP complexes with sgRNA. In addition, our recombinant RNP delivery followed a standard best practice for such experiments by culturing cells with stimulation beads post-electroporation[64], which may have increased susceptibility to editing. Thus, evaluating potential benefits of recipient cells stimulation strategies and alternative dosing regimens (including co-culture of EV producer and recipient cells in vitro) may present interesting avenues for future exploration. In the specific HIV application contemplated, conversion of even a limited pool of T cells to resist HIV infection could confer therapeutic benefits[74]. EVs have been explored for potential utility in HIV treatment through approaches such as Cas9-mediated excision of proviruses in microglial cells[69], repressing viral replication with zinc finger-fused methyltransferases[67] or killing of infected cells using HIV Env-targeted vesicles[75], but these preliminary demonstrations have not yet been developed into methods for achieving targeted delivery and treatment of T cells using a clinically translatable approach. Another important finding is that while exact editing efficiencies varied across donors and EV doses (a pattern observed with Cas9 RNP delivery by other methods[61]), the overall trends we observed were highly conserved when controlling for these effects, showing repeatability. These results are particularly exciting when noting that the quantified efficiencies are limited by Cas9-mediated cleavage and DNA repair rates, such that we are certainly underestimating the number of functional delivery events, and other cargo types and mechanisms might confer even greater rates of functional delivery.

A surprising finding is that CD2 engagement, by either recombinant antibody or EV-displayed antibody, enhanced functional exosome-mediated delivery in vitro, although no comparable benefit for MV-mediated delivery was observed. This combination of effects is not explained by known features of CD2/T-cell biology, although it could be related to findings that ligand engagement triggers CD2 internalization[34]. While scFv-displaying vesicles of both types specifically bound CD2 and were internalized to some degree, there may exist a difference in intracellular trafficking and fusion between the two vesicle populations. For example, CD2-binding-mediated trafficking might favour fusion over native uptake pathways in a way that differentially favours exosomes. Overall, even though target-cell binding and uptake were generally more efficient for MVs than for exosomes, functional delivery of cargo (which requires fusion of EV and recipient-cell membranes) was generally more efficient for exosomes. This somewhat counterintuitive trend is not necessarily a contradiction and may indicate important roles for EV components (such as naturally loaded proteins and lipids) or physical properties that differ across EV subtypes. These phenomena warrant further study to elucidate underlying mechanisms.

A key feature of this study is the selection of methods that avoid artefacts found in EV studies. One general and often overlooked artefact with EV functional delivery experiments is the risk of transfer of residual producer cell transfection reagent; particles from cells transfected with lipoplexes can mediate functional effects erroneously attributed to EVs[24]. We minimized such risks by using a transfection method that is unlikely to transfer plasmids to T cells. Key comparative observations (for example, differences in functional delivery by viral glycoprotein choice) support our interpretation that we quantified true EV-mediated delivery.

The technologies used here are generalizable and amenable to large-scale production and biomanufacturing. Our strategy of genetically programming the self-assembly of multifunctional particles avoids the need for post-collection chemical modification that necessitates further purification and lower EV yields and may incur regulatory challenges. Although we used transient transfections for some transgenes (for example, viral glycoproteins that cannot be constitutively expressed due to toxicity), such genes are regularly expressed from inducible promoters for production of biologics[76,77]. We anticipate that the integrated tools developed here for EV targeting, cargo loading and vesicle fusion will be widely applicable for a range of applications and targets, providing a flexible suite of technologies for engineering EV therapeutics.

Methods

Plasmid construction

Plasmids were constructed using standard molecular biology techniques. Codon optimization was performed using the GeneArt gene synthesis tool (Thermo Fisher). Polymerase chain reaction (PCR) was performed using Phusion DNA polymerase (New England Biolabs, NEB), and plasmid assembly was performed via restriction enzyme cloning. Plasmids were transformed into TOP10 competent *Escherichia coli* (Thermo Fisher) and grown at 37 °C.

Plasmid backbones

A modified pcDNA3.1 (Thermo Fisher V87020) was used to generate a general expression vector. Briefly, the hygromycin resistance gene and SV40 promoter were removed, leaving the SV40 origin of replication and poly(A) signal intact. The BsaI sites in the AmpR gene and 5′-UTR and the BpiI site in the bGH poly(A) signal were mutated. The lentiviral vector pGIPZ (Open Biosystems) was obtained through the Northwestern High Throughput Analysis Laboratory. plentiCRISPRv2 was a gift from Feng Zhang[78] (Addgene plasmid number 52961).

Plasmid source vectors

Fluorescent proteins enhanced blue fluorescent protein 2 (EBFP2), EYFP and dTomato were sourced from Addgene vectors (plasmid numbers 14893, 58855 and 18917, respectively) gifted by Robert Campbell[79],

Joshua Leonard[80] and Scott Sternson[81]. The plasmid encoding human CXCR4 (Addgene 98942) was a gift from Erik Procko[82]. dsRedExpress2 was purchased from Clontech/Takara. Monomeric teal fluorescent protein 1 (mTFP1) was synthesized by Thermo Fisher. psPAX2 and pMD2.G were gifts from William Miller. The anti-CD2 scFv was synthesized from a previously published scFv sequence derived from monoclonal antibody 9.6[33], and the PDGFR transmembrane domain was sourced from a pDisplay system vector (Addgene plasmid number 61556, gifted by Robert Campbell)[83]. The C1C2 domain sequence was provided by Natalie Tigue[30] and synthesized by Thermo Fisher. Constitutively active Cx43 and SLAM were synthesized by Thermo Fisher from Uniprot sequences P17302 CXA1_HUMAN and Q13291-1 SLAF1_HUMAN isoform 1, respectively. Plasmids encoding the measles virus glycoproteins were gifts from Isabelle Clerc, Thomas Hope and Richard D'Aquila[54]. pX330 encoding Cas9 was gifted by Erik Sontheimer (University of Massachusetts), originally sourced from Addgene plasmid number 42230 gifted by Feng Zhang[84]. The CXCR4 sgRNA sequence was provided by Judd Hultquist and is as follows: GAAGCGTGATGACAAAGAGG[61]. ABI and PYL domains[47] were codon optimized and synthesized by Thermo Fisher and Integrated DNA Technologies (IDT), respectively.

Plasmid preparation

Bacteria were grown overnight in 100 ml Luria broth + ampicillin cultures for 12–14 h. Cultures were spun at 3,000 *g* for 10 min to pellet the bacteria, and pellets were resuspended and incubated for 30 min in 4 ml of 25 mM Tris pH 8.0, 10 mM ethylenediaminetetraacetic acid (EDTA), 15% sucrose, and 5 mg ml^{-1} lysozyme. Bacteria were lysed for 15 min in 8 ml of 0.2 M NaOH and 1% sodium dodecyl sulfate (SDS), followed by a 15 min neutralization in 5 ml of 3 M sodium acetate (pH 5.2). The precipitate was pelleted at 9,000 *g* for 20 min, and the supernatant was filtered through cheese cloth and incubated for 1–3 h at 37 °C with 3 µl of 10 mg ml^{-1} RNAse A (Thermo Fisher). Samples were extracted with 5 ml phenol chloroform, and the aqueous layer was recovered after centrifugation at 7,500 *g* for 20 min. A second phenol chloroform extraction was performed with 7 ml solvent. About 0.7 volume isopropanol was added to the recovered supernatant, and samples were inverted and incubated at room temperature for 10 min before centrifugation at 9,000 *g* for 20 min to pellet the DNA mixture. Pellets were briefly dried and resuspended in 1 ml of 6.5% polyethylene glycol 20,000 and 0.4 M NaCl. DNA was incubated on ice overnight and pelleted at 21,000 *g* for 20 min. The supernatant was removed, and pellets were washed in cold absolute ethanol and dried at 37 °C before resuspension in Tris-EDTA (TE) buffer (10 mM Tris, 1 mM EDTA, pH 8.0). DNA was diluted to 1 µg $µl^{-1}$ using a Nanodrop 2000 (Thermo Fisher).

Cell culture

HEK293FT cells (Thermo Fisher R70007) were cultured in Dulbecco's modified Eagle medium (DMEM, Gibco 31600-091) supplemented with 10% fetal bovine serum (FBS) (Gibco 16140-071), 1% penicillin–streptomycin (Gibco 15140-122) and 4 mM additional L-glutamine (Gibco 25030-081). Jurkat T cells (ATCC TIB-152) were cultured in Roswell Park Memorial Institute medium (RPMI 1640, Gibco 31800-105) supplemented with 10% FBS, 1% penicillin–streptomycin, and 4 mM L-glutamine. Sublines generated from these cell lines were cultured in the same way. Cells were subcultured at a 1:5 or 1:10 ratio every 2–3 days, using trypsin–EDTA (Gibco 25300-054) to remove adherent cells from the plate. Lenti-X cells (Takara) were cultured the same way with additional 1 mM sodium pyruvate (Thermo Fisher 11360-070). Primary human $CD4^+$ T cells were cultured in RPMI supplemented with 10% FBS, 1% penicillin–streptomycin, 5 mM (4-(2-hydroxyethyl)-1-piperazineethanesulfonic acid) HEPES, 5 mM sodium pyruvate and 20 U ml^{-1} interleukin-2 (IL-2) (added fresh at the time of use). Cells were maintained at 37 °C at 5% CO_2. HEK293FT and Jurkat cells tested negative for mycoplasma with the MycoAlert Mycoplasma Detection Kit (Lonza LT07-318).

Transfection

For transfection of HEK293FT cells and derived cell lines in 15 cm dishes for EV packaging, cells were plated at a density of 18×10^6 cells per dish (1×10^6 cells per ml) 6–12 h before transfection. Cells were transfected with 30 µg DNA plus 1 µg of a fluorescent transfection control via the calcium phosphate method. Plasmid DNA was mixed with 2 M $CaCl_2$ (final concentration 0.3 M) and added to a 2× HEPES-buffered saline solution (280 mM NaCl, 0.05 M HEPES, 1.5 mM Na_2HPO_4) dropwise in a 1:1 ratio and mixed seven times by pipetting. The transfection solution was incubated for 3 min, mixed eight times by pipetting and added gently to the side of the plate. For transfection of HEK293FT cells in 10 cm dishes for EV packaging, cells were plated at a density of 5×10^6 cells per dish (6.25×10^5 cells per ml) and transfected with 20 µg DNA plus 1 µg transfection control as described above, adding transfection mixture dropwise to the dish. Lenti-X cells were transfected in 10 cm dishes in the same manner but were plated 24 h before transfection as per the manufacturer's recommendation (Takara). For transfection of HEK293FT cells in 24-well plates, cells were plated at a density of 1.7×10^5 cells per well (3.4×10^5 cells per ml) and transfected with 200 µg DNA as described above, adding transfection mixture dropwise to the well. The medium was changed 12–16 h later. Jurkat lipofectamine transfections were performed according to the manufacturer's protocol.

Cell line generation

To generate lentivirus, HEK293FT or Lenti-X cells were plated in 10 cm dishes at a density of 5×10^6 cells per dish (6.25×10^5 cells per ml). About 6–12 h later for HEK293FT or 24 h later for Lenti-X, cells were transfected with 10 µg of viral vector, 8 µg psPAX2 second generation lentiviral packaging plasmid, and 3 µg pMD2.G VSV- G plasmid via calcium phosphate transfection as described above. The medium was changed 12–16 h later. At 28 h post medium change, lentivirus was collected from the conditioned medium. The medium was centrifuged at 500 *g* for 2 min to clear cells, and the supernatant was filtered through a 0.45 µm pore filter (VWR). Lentivirus was concentrated from the filtered supernatant by ultracentrifugation in Ultra Clear tubes (Beckman Coulter 344059) at 100,420 *g* at 4 °C in a Beckman Coulter Optima L-80 XP ultracentrifuge using an SW41Ti rotor. The supernatant was aspirated, leaving virus in ~100 µl final volume, and concentrated lentivirus was left on ice for at least 30 min before resuspension, then used to transduce ~1×10^5 cells, plated either at the time of transduction or on the day before. When appropriate, drug selection began 2 days post transduction, using antibiotic concentrations of 1 µg ml^{-1} puromycin (Invitrogen ant-pr) and 10 µg ml^{-1} blasticidin (Alfa Aesar J61883) on HEK293FT cells or 0.2 µg ml^{-1} puromycin and 2 µg ml^{-1} blasticidin on Jurkat cells. Cells were kept in antibiotics for at least 2 weeks with subculturing every 1 to 2 days.

Sorting of Cas9 reporter lines

Cells were prepared for fluorescence-activated cell sorting (FACS) by resuspending in either DMEM or RPMI, as appropriate, supplemented with 10% FBS, 25 mM HEPES and 100 µg ml^{-1} gentamycin (Amresco 0304) at a concentration of 1×10^7 cells per ml. Cells were sorted for the highest mTFP1 expressors (top 10% or less) lacking any dTomato expression on a BD FacsAria IIu using a 488 nm laser (530/30 filter) and a 562 nm laser (582/15 filter). Cells were collected in DMEM or RPMI, as appropriate, supplemented with 20% FBS, 25 mM HEPES and 100 µg ml^{-1} gentamycin. Cells were spun down and resuspended in normal growth medium with 100 µg ml^{-1} gentamycin for recovery.

EV production, isolation and characterization

EV producer cell lines were plated in 10 or 15 cm dishes and transfected the same day by the calcium phostomycinphate method where appropriate. The medium was changed to EV-depleted medium the following morning. EV-depleted medium was made by supplementing DMEM with 10% exosome-depleted FBS (Gibco A27208-01), 1%

penicillin–streptomycin and 4 mM L-glutamine. EVs were collected from the conditioned medium 24–36 h post medium change by differential centrifugation as previously described[36,37]. Briefly, conditioned medium was cleared of debris by centrifugation at 300 *g* for 10 min to remove cells followed by centrifugation at 2,000 *g* for 20 min to remove dead cells and apoptotic bodies. The supernatant was centrifuged at 15,000 *g* for 30 min in a Beckman Coulter Avanti J-26XP centrifuge with a J-LITE JLA 16.25 rotor to pellet MVs. The supernatant was collected and exosomes pelleted by ultracentrifugation at 120,416 *g* for 135 min in a Beckman Coulter Optima L-80 XP ultracentrifuge with an SW41 Ti rotor, using polypropylene ultracentrifuge tubes (Beckman Coulter 331372). All centrifugation steps were performed at 4 °C. EV pellets were left in ~100–200 µl of conditioned medium and incubated on ice for at least 30 min after supernatant removal before resuspension. EV concentration was determined by NanoSight analysis. Samples were diluted in phosphate-buffered saline (PBS) to concentrations on the order of 10^8 particles per ml for analysis. NanoSight analysis was performed on an NS300 (Malvern), software version 3.4. Three 30 s videos were acquired per sample using a 642 nm laser on a camera level of 14, an infusion rate of 30 and a detection threshold of 7. Default settings were used for the blur, minimum track length and minimum expected particle size. EV concentrations were defined as the mean of the concentrations calculated from each video. Size distributions were generated by the software. For transmission electron microscopy (TEM), samples were fixed for 10 min in Eppendorf tubes by adding 65 µl of 4% PFA to 200 µl of EVs. About 15 µl of fixed suspension was pipetted onto a plasma cleaned (PELCO easiGlow), formvar/carbon-coated grid (EMS 300 mesh). After 10 min, the solution was removed by wicking with a wedge of filter paper, then washed by inverting the grid onto a drop of buffer for 30 s twice, followed with deionized water (diH_2O) once. A 2% uranyl acetate (Ted Pella) stain was applied twice and wicked after 30 s. Grids were allowed dry before storing in a grid box until use. Grids were imaged in a JEOL JEM 1230 TEM (JEOL USA) with a 100 KV accelerating voltage. Data were acquired with an Orius SC1000 CCD camera (Gatan). EVs were stored on ice and used within 10 days or stored at −80 °C for long-term preservation.

Immunoblotting

For western blot analysis, cells were lysed in radioimmunoprecipitation assay buffer (150 mM NaCl, 50 mM Tris–HCl pH 8.0, 1% Triton X-100, 05% sodium deoxycholate, 0.1% SDS and one protease inhibitor cocktail tablet (Pierce PIA32953) per 10 ml) and incubated on ice for 30 min. Lysates were cleared by centrifugation at 12,000 *g* for 20 min at 4 °C, and the supernatant was collected. Protein concentration was determined by bicinchoninic acid assay (Pierce) according to the manufacturer's instructions. Samples were normalized by protein content ranging from 1 to 2 µg (for cell lysates) or by vesicle count ranging from 1×10^7 to 6×10^8 (for EVs). EV normalization by vesicle count was chosen to reduce the risk of artefacts associated with protein-based normalization due to contamination of EV preps with bovine serum albumin (BSA). Samples were heated in Laemmli buffer (60 mM Tris–HCl pH 6.8, 10% glycerol, 2% SDS, 100 mM dithiothreitol, 0.01% bromophenol blue) at 70 °C (for membrane-bound scFv and calnexin) or 98 °C (for Cas9, CD9, CD81 and Alix) for 10 min. Samples were loaded onto 4–15% polyacrylamide gradient Mini-PROTEAN TGX precast protein gels (Bio-Rad) and run at 50 V for 10 min followed by 100 V for 1 h. Protein was transferred to a polyvinylidene difluoride membrane (Bio-Rad) at 100 V for 45 min. For anti-FLAG blots, membranes were blocked in 3% milk in tris-buffered saline (TBS; 50 mM Tris, 138 mM NaCl, 2.7 mM KCl, pH 8.0) for 30 min. Membranes were washed once in TBS for 5 min then incubated in primary anti-FLAG antibody (Sigma F1804) diluted 1:1,000 in 3% milk in TBS overnight at 4 °C. Membranes were washed once for 5 min in TBS and twice in TBST 1 (50 mM Tris, 138 mM NaCl, 2.7 mM KCl, 0.05% Tween 20, pH 8.0) for 5 min each before secondary antibody staining. For all other blots, membranes were blocked in 5% milk in TBST 2 (50 mM Tris, 150 mM NaCl, 0.1% Tween 20, pH 7.6) for 1 h. Membranes were incubated in primary antibody diluted in 5% milk in TBST 2 overnight at 4 °C. Primary antibodies include anti-HA (Cell Signaling Technology 377245 C29F4, 1:1000), anti-CD9 (Santa Cruz Biotechnology sc-13118, 1:500), anti-CD81 (Santa Cruz Biotechnology sc-23962, 1:500, run in non-reducing conditions), anti-Alix (Abcam Ab117600, 1:500), anti-calnexin (Abcam Ab22595, 1:1,000) and anti-Cas9 (Cell Signaling Technology 7A9-3A3, 1:1,000). Membranes were washed three times in TBST 2 for 5 min each before secondary antibody staining. HRP-conjugated anti-mouse (Cell Signaling Technology 7076) and anti-rabbit (Invitrogen 32460) secondary antibodies were diluted 1:3,000 in 5% milk in TBST 2. Membranes were incubated in secondary antibody at room temperature for 1 h, then washed three times in TBST 2 (5 min washes). Membranes were probed with Clarity Western ECL Substrate (Bio-Rad) and either exposed to film, which was developed and scanned, or imaged using an Azure c280 imager. Images were cropped using Adobe Illustrator. No other image processing was used.

Surface immunoblotting

Cells were transferred to FACS tubes (adherent cells were collected using FACS buffer (PBS pH 7.4 with 0.05% BSA and 2 mM EDTA) before staining) with 1 ml of FACS buffer and centrifuged at 150 *g* for 5 min. The supernatant was decanted, and cells were resuspended in 50 µl of FACS buffer. 10 µl of human IgG (Thermo Fisher 027102) was added, cells were flicked to mix and were incubated at 4 °C for 5 min. Conjugated primary antibody was then added at the manufacturer's recommended dilution, and cells were flicked to mix and incubated at 4 °C for 30 min. Cells were then washed three times with 1 ml of FACS buffer, centrifuging at 150 *g* for 5 min and decanting the supernatant after each wash. Cells were resuspended in two drops of FACS buffer before flow cytometry. For Miltenyi Biotec antibodies, cells were stained at 4 °C for 15 min without blocking and were washed once before flow cytometry, as per manufacturer's protocol. Antibodies used in this study were as follows: anti-FLAG–APC (Abcam ab72569), anti-CD2–APC (R&D Systems FAB18561A), anti-CXCR4 (Miltenyi REA649, 130-117-354), anti-CD25–PE (Miltenyi REA945, 130-115-628) and anti-SLAM–PE (Miltenyi REA151, 130-123-970). Anti-mouse IgG1–APC (R&D Systems IC002A) and anti-human IgG1–PE (Miltenyi REA293, 130-113-438) were used as isotype controls where appropriate.

EV binding and uptake experiments

Jurkat T cells or primary human $CD4^+$ T cells were incubated with EVs at an EV-to-cell ratio of 100,000:1 (typically 1×10^{10} EVs per 1×10^5 cells) unless otherwise indicated. For Jurkats, cells were plated in a 48-well plate with 300 µl total volume. For primary T cells, cells were plated in a 96-well plate with 200 µl total volume. Cells were plated at the time of EV addition, and wells were brought to the appropriate volume with RPMI. For binding experiments, cells were incubated for 2 h at 37 °C unless otherwise indicated, then washed three times in FACS buffer, centrifuging at 150 *g* for 5 min for Jurkat cells or 400 *g* for 3 min for primary T cells. Cells were resuspended in one drop of FACS buffer before flow cytometry. To adsorb EVs to aldehyde/sulfate latex beads (Thermo Fisher), EVs were mixed with beads at a ratio of 1×10^9 EVs per 2 µl beads diluted 1:10 in PBS. Volumes were normalized across samples with PBS, and beads and EVs were incubated for 15 min at room temperature. Samples were then brought to 200 µl with PBS and allowed to incubate for 2 h at room temperature while rocking. Cells were blocked with an anti-CD2 antibody binding the same epitope as the scFv (Beckman Coulter A60794) or with blank EVs for 1 h at 37 °C before EV incubation where indicated. For EV uptake experiments with viral glycoproteins, cells were incubated with EVs for 16 h at 37 °C. To prepare for analysis, cells were washed twice in PBS and incubated with two drops of trypsin–EDTA for 5 min at 37 °C to remove surface-bound vesicles. Cells were washed with RPMI to quench the trypsin, then washed twice more with FACS buffer before analysis.

Analytical flow cytometry and analysis

Flow cytometry was performed on a BD LSR Fortessa Special Order Research Product using the 562 nm laser for dTomato (582/15 filter), the 488 nm laser for EYFP (530/30 filter) and the 488 nm and 405 nm lasers for mTFP1 (530/30 filter and 525/50 filter, respectively). Approximately 10,000 live cells were collected per sample for analysis. Data were analysed using FlowJo v10 (FlowJo, LLC). Briefly, cells were identified using an forward scatter area (FSC-A) versus side scatter area (SSC-A) plot and gated for singlets using an FSC-A versus forward scatter height (FSC-H) plot (Supplementary Fig. 19). In transfection experiments, transfected cells were identified by fluorescence attributable to the transfection control by gating using a non-fluorescent control (Supplementary Fig. 20). Fluorescence data were compensated for spectral bleed-through where appropriate. Mean fluorescence intensity of single-cell samples was exported and averaged across three biological replicates. Autofluorescence from untreated cells was subtracted from other samples. Standard error of the mean was propagated through calculations. Where indicated, 9 peak Ultra Rainbow Calibration Particles (Spherotech URCP-100-2H) were used to generate a calibration curve to convert fluorescence into absolute fluorescence units.

Confocal microscopy

Cells were transfected via the calcium phosphate method on poly L-lysine coated glass coverslips and mounted on glass slides for imaging. Microscopy images were taken on Leica SP5 II laser scanning confocal microscope using a ×100 oil-immersion objective. Bright-field images were acquired at a photomultiplier tube (PMT) setting of 443.0 V. A 514 nm laser at 20% intensity and 94% smart gain was used for fluorescence excitation. Emission spectra were captured from 520–540 nm using an HyD sensor. Images were captured at 512 × 512 resolution at a scanning speed of 400 Hz. Pseudocoloured fluorescence images were contrast-adjusted in ImageJ v1.53f51 such that 4% of pixels were saturated.

Affinity chromatography

Affinity chromatography isolation was performed as previously reported[50]. Briefly, an anti-FLAG affinity column was prepared by loading anti-FLAG M2 affinity gel (Sigma A2220-1ML) in a 4 ml 1 × 5 cm glass column (Bio-Rad) and drained via gravity flow. The column was washed with 5 ml TBS (50 mM Tris–HCl, 150 mM NaCl, pH 7.5) and equilibrated with three sequential 1 ml washes with regeneration buffer (0.1 M glycine–HCl, pH 3.5), followed by a 5 ml wash of TBS. Concentrated EVs were loaded onto the top of the column and chased with 1–2 ml of TBS. The column was incubated with EVs for 5 min before continuing. The flow-through was then re-loaded onto the column such that the EV-containing medium passed through the matrix five times. The column was washed with 10 ml TBS before elution. EVs were eluted with 2.5 ml elution buffer (100 μg ml^{-1} 3× FLAG peptide (Sigma F4799-4MG) in TBS), which was incubated on the column for 5–10 min after the void fraction was drained (~1 ml). Five fractions of EVs were collected in 0.5 ml fractions (approximately 8 drops off the column per fraction). The column was regenerated with three sequential 1 ml washes with regeneration buffer and stored at 4 °C in storage buffer (50% glycerol, 0.02% sodium azide in TBS).

Cas9 in vitro cleavage assays

EVs were produced as described above with components transiently transfected in 10 cm dishes with the following DNA ratios: 6 μg anti-CD2 scFv, 9 μg Cas9 vector, 5 μg sgRNA vector and 1 μg mTFP1 transfection control. EVs were lysed by incubation with mammalian protein extraction reagent (Thermo Fisher) for 10 min at room temperature (20–23 °C) with gentle agitation. About 200 ng of linearized target plasmid template was added to vesicles with Cas9 reagent buffer (IDT, Alt-R CRISPR–Cas9 System), and samples were incubated at 37 °C for 1 h. Proteinase K (Thermo Fisher) was added to samples at 1 μl per 10 μl of reaction mixture and incubated at 55 °C for 10 min. Samples were run on a 1% agarose gel stained with SYBR safe (Thermo Fisher) and imaged using a BioDoc-It imaging system (VWR).

Primary CD4$^+$ T-cell isolation, culture and activation

Peripheral blood mononuclear cells (PBMCs) were isolated by density gradient centrifugation using Ficoll-Paque Plus (GE Health Care, number 17-1440-02). PBMCs were washed with PBS three times to remove platelets and suspended at a final concentration of 5×10^8 cells per ml in PBS, 0.5% BSA and 2 mM EDTA. Bulk CD4$^+$ T cells were subsequently isolated from PBMCs by magnetic negative selection using an EasySep Human CD4$^+$ T Cell Isolation Kit (STEMCELL, per manufacturer's instructions). Isolated CD4$^+$ T cells were suspended in RPMI-1640 (Gibco) supplemented with 5 mM HEPES (Corning), 50 μg ml^{-1} penicillin–streptomycin (Corning), 5 mM sodium pyruvate (Corning) and 10% FBS (Gibco). The medium was supplemented with 20 IU ml^{-1} IL-2 (Miltenyi) immediately before use. For activation, bulk CD4$^+$ T cells were immediately plated on anti-CD3-coated plates (coated for 12 h at 4 °C with 20 μg ml^{-1} anti-CD3 (UCHT1, Tonbo Biosciences)) in the presence of 5 μg ml^{-1} soluble anti-CD28 (CD28.2, Tonbo Biosciences). Cells were stimulated for 72 h at 37 °C and 5% CO_2. After stimulation, cell purity and activation were verified by CD4/CD25 immunostaining and flow cytometry as previously described[61].

EV functional delivery experiments

EVs were produced as described above with components transiently transfected in 10 cm dishes with the following DNA ratios: 6 μg anti-CD2 scFv, 9 μg dual Cas9 and sgRNA vector, either 2.5 μg each of measles virus glycoproteins H/F or 3 μg VSV-G with 2 μg filler promoterless pcDNA, and 1 μg mTFP1 transfection control. For generation of vesicles lacking the scFv, a PDGFR-bound 3× FLAG tag construct in the same vector backbone was transfected at the same plasmid copy number in place of the scFv. EVs were delivered to primary human CD4$^+$ T cells as described above. Cells were cultured in the presence of EVs for 6 days, adding fresh supplemental RPMI and IL-2 every 2–3 days. For repeat dose administration, 100 μl of medium was carefully removed from the top of each well and replaced with 100 μl fresh EVs and media. Cells were collected on day 6 and washed with PBS by centrifugation at 400 *g* for 3 min at 4 °C to pellet. Cells were resuspended in 100 μl QuickExtract DNA Extract Solution (Lucigen QE9050), and genomic DNA was collected according to the manufacturer's protocol. Briefly, samples were vortexed for 15 s, heated at 65 °C for 6 min, vortexed for 15 s and heated at 98 °C for 2 min. DNA was stored at −80 °C.

Cas9 loading quantification

Cas9-containing EV samples were compared on a western blot to a Cas9 standard curve generated using purified, recombinant *S. pyogenes* Cas9 (IDT, 1081058) diluted to specified numbers of molecules. Non-saturated band intensities were quantified using ImageJ, and Cas9 loading was calculated using a linear regression of the standard curve in the linear range of signal.

Cas9 RNP electroporation

Electroporation was performed using the Amaxa P3 Primary Cell 96-well Nucleofector kit and 4D-Nucleofecter (Lonza). Recombinant *S. pyogenes* Cas9 protein containing a C-terminal HA tag and two NLS peptides was expressed and purified as previously described[85] and obtained from the QB3 Macrolab (University of California, Berkeley). Guide RNAs were introduced as a pair of CRISPR RNA (crRNA) and trans-activating crRNA (tracrRNA). Each crRNA and the tracrRNA was chemically synthesized (Horizon Biosciences). To generate the targeted Cas9 RNP dilution series, CXCR4-targeted crRNA was mixed with a non-targeted crRNA at 1×, 5×, 10×, 50×, 100×, 500× and 1,000× dilutions; this strategy was selected to avoid possible confounding effects of protein instability at low concentrations and possible stabilization of

Cas9 by binding to guide RNA. Cas9 RNPs were prepared fresh for each experiment. The crRNA and tracrRNA were first mixed 1:1 and incubated for 30 min at 37 °C to generate 40 µM crRNA:tracrRNA duplexes. An equal volume of 40 µM *S. pyogenes* Cas9–NLS was slowly added to the crRNA:tracrRNA and incubated for 15 min at 37 °C to generate 20 µM Cas9 RNPs. For each reaction, roughly 1×10^5 stimulated T cells were pelleted and resuspended in 20 µl P3 buffer. About 3.5 µl of 20 µM Cas9 RNP mix (corresponding to ~4.2×10^{13} total Cas9 molecules) was added directly to these cells, and the entire volume was transferred to the 96-well reaction cuvette. Cells were electroporated using program EH-115 on the Amaxa 4D-Nucleofector (Lonza). About 100 µl pre-warmed, complete RPMI was added to each well, and the cells were allowed to recover for 30 min at 37 °C. Cells were then restimulated with a T Cell Activation/Expansion kit (Miltenyi).

HTS library generation

Approximately 100 ng genomic DNA was used as a template in the first-round PCR amplification. The CXCR4 region of interest was amplified with the following primers: F1: 5′ ACA CTC TTT CCC TAC ACG CTC TTC CGA TCT NNN NNG AGA AGC ATG ACG GAC AAG TAC AG 3′; R1: 5′ GTG ACT GGA GTT CAG ACG TGT GCT CTT CCG ATC TNN NNN TCC CAA AGT ACC AGT TTG CCA C 3′. The PCR protocol was as follows: 98 °C 3 min, (98 °C 15 s, 65 °C 30 s, 72 °C 3 s) × 15, 72 °C 5 min, 4 °C 5 min. PCR products were purified using MagJET beads (Thermo Fisher K2821) and used as templates in a second-round PCR amplification with the following primers: F2: 5′ AAT GAT ACG GCG ACC GAG ATC TAC ACT CTT TCC CTA CAC GAC GCT CTT CCG ATC T 3′; R2: 5′ CAA GCA GAA GAC GGC ATA CGA GAT-Index-GTG ACT GGA GTT CAG ACG TGT GCT C 3′. The PCR cycles were as follows: 98 °C 3 min, (98 °C 15 s, 69 °C 30 s, 72 °C 5 s) × 20, 72 °C 5 min, 4 °C 5 min. PCR products were again purified using MagJET beads before HTS. Both first- and second-round PCRs were run with primer concentrations of 200 nM and Phusion DNA polymerase.

HTS

Genomic DNA sample concentrations were measured on a Qubit using an HS dsDNA kit and pooled in libraries with equimolar concentrations. Libraries were diluted to 4 nM in serial dilutions. Libraries and PhiX were denatured with NaOH according to the Illumina MiSeq guide and diluted to 14 pM. Reaction mixtures consisted of 8% PhiX and 92% library. Samples were run on an Illumina MiSeq using a MiSeq Reagent Kit v3, collecting paired-end reads. Data were analysed using custom code developed by 496code ('Data availability' and 'Code availability'). The overall strategy for analysing these data is summarized in Supplementary Note 1.

Statistical analysis

Statistical details are described in the figure legends. Unless otherwise stated, three independent biological replicates (cells) or technical replicates (beads) were analysed per condition, and the mean fluorescence intensity of approximately 10,000 live single cells or beads were analysed per sample. Unless otherwise indicated, error bars represent the standard error of the mean. Pairwise comparisons were made using two-tailed Student's *t*-tests in Excel with the null hypothesis that the two samples were equal. The significance threshold was set to 0.05. Tests were followed by a Benjamini–Hochberg procedure applied within each panel of a given figure to decrease the false discovery rate.

Reporting summary

Further information on research design is available in the Nature Portfolio Reporting Summary linked to this article.

Data availability

All reported experimental data and plasmid maps for all plasmids generated in this study are freely available at Zenodo (https://doi.org/10.5281/zenodo.10022991). Key plasmids used in this study are distributed by Addgene, with complete and annotated GenBank files available at https://www.addgene.org/Joshua_Leonard. The raw and analysed datasets generated during the study are available for research purposes from the corresponding author on reasonable request.

Code availability

The code for analysing HTS data is available at https://github.com/leonardlab/GEMINI-HTS under an open-source license.

References

1. Sadelain, M., Rivière, I. & Riddell, S. Therapeutic T cell engineering. *Nature* **545**, 423–431 (2017).
2. Yin, C. et al. In vivo excision of HIV-1 provirus by saCas9 and multiplex single-guide RNAs in animal models. *Mol. Ther.* **25**, 1168–1186 (2017).
3. Kaminski, R. et al. Excision of HIV-1 DNA by gene editing: a proof-of-concept in vivo study. *Gene Ther.* **23**, 690–695 (2016).
4. Dash, P. K. et al. Sequential LASER ART and CRISPR treatments eliminate HIV-1 in a subset of infected humanized mice. *Nat. Commun.* **10**, 2753 (2019).
5. Louis Jeune, V., Joergensen, J. A., Hajjar, R. J. & Weber, T. Pre-existing anti-adeno-associated virus antibodies as a challenge in AAV gene therapy. *Hum. Gene Ther. Methods* **24**, 59–67 (2013).
6. Zincarelli, C., Soltys, S., Rengo, G. & Rabinowitz, J. E. Analysis of AAV serotypes 1–9 mediated gene expression and tropism in mice after systemic injection. *Mol. Ther.* **16**, 1073–1080 (2008).
7. Hamilton, J. R. et al. Targeted delivery of CRISPR–Cas9 and transgenes enables complex immune cell engineering. *Cell Rep.* **35**, 109207 (2021).
8. Banskota, S. et al. Engineered virus-like particles for efficient in vivo delivery of therapeutic proteins. *Cell* **185**, 250–265 (2022).
9. Segel, M. et al. Mammalian retrovirus-like protein PEG10 packages its own mRNA and can be pseudotyped for mRNA delivery. *Science* **373**, 882–889 (2021).
10. Otten, G. R. et al. Potent immunogenicity of an HIV-1 gag-pol fusion DNA vaccine delivered by in vivo electroporation. *Vaccine* **24**, 4503–4509 (2006).
11. Rurik, J. G. et al. CAR T cells produced in vivo to treat cardiac injury. *Science* **375**, 91–96 (2022).
12. Luther, D. C., Lee, Y. W., Nagaraj, H., Scaletti, F. & Rotello, V. M. Delivery approaches for CRISPR/Cas9 therapeutics in vivo: advances and challenges. *Expert Opin. Drug Deliv.* **15**, 905–913 (2018).
13. Liu, C., Zhang, L., Liu, H. & Cheng, K. Delivery strategies of the CRISPR–Cas9 gene-editing system for therapeutic applications. *J. Control. Release* **266**, 17–26 (2017).
14. Dardalhon, V. et al. Lentivirus-mediated gene transfer in primary T cells is enhanced by a central DNA flap. *Gene Ther.* **8**, 190–198 (2001).
15. Valadi, H. et al. Exosome-mediated transfer of mRNAs and microRNAs is a novel mechanism of genetic exchange between cells. *Nat. Cell Biol.* **9**, 654–659 (2007).
16. Soderberg, A., Barral, A. M., Soderstrom, M., Sander, B. & Rosen, A. Redox-signaling transmitted in trans to neighboring cells by melanoma-derived TNF-containing exosomes. *Free Radic. Biol. Med.* **43**, 90–99 (2007).
17. Alvarez-Erviti, L. et al. Delivery of siRNA to the mouse brain by systemic injection of targeted exosomes. *Nat. Biotechnol.* **29**, 341–345 (2011).
18. Arslan, F. et al. Mesenchymal stem cell-derived exosomes increase ATP levels, decrease oxidative stress and activate PI3K/Akt pathway to enhance myocardial viability and prevent adverse remodeling after myocardial ischemia/reperfusion injury. *Stem Cell Res.* **10**, 301–312 (2013).

19. Ohno, S. et al. Systemically injected exosomes targeted to EGFR deliver antitumor microRNA to breast cancer cells. *Mol. Ther.* **21**, 185–191 (2013).
20. Kojima, R. et al. Designer exosomes produced by implanted cells intracerebrally deliver therapeutic cargo for Parkinson's disease treatment. *Nat. Commun.* **9**, 1305 (2018).
21. He, C. et al. Epithelial cell-derived microvesicles: a safe delivery platform of CRISPR/Cas9 conferring synergistic anti-tumor effect with sorafenib. *Exp. Cell. Res.* **392**, 112040 (2020).
22. Chen, R. et al. Friend or foe? Evidence indicates endogenous exosomes can deliver functional gRNA and Cas9 protein. *Small* **15**, e1902686 (2019).
23. Yao, X. et al. Engineered extracellular vesicles as versatile ribonucleoprotein delivery vehicles for efficient and safe CRISPR genome editing. *J. Extracell. Vesicles* **10**, e12076 (2021).
24. McConnell, R., Y. M. & Finn, J. In *International Society for Extracellular Vesicles* (Taylor & Francis Online, 2022).
25. Kooijmans, S. A. et al. Electroporation-induced siRNA precipitation obscures the efficiency of siRNA loading into extracellular vesicles. *J. Control. Release* **172**, 229–238 (2013).
26. Théry, C. et al. Minimal information for studies of extracellular vesicles 2018 (MISEV2018): a position statement of the International Society for Extracellular Vesicles and update of the MISEV2014 guidelines. *J. Extracell. Vesicles* **7**, 1535750 (2018).
27. Knipping, F. et al. Disruption of HIV-1 co-receptors CCR5 and CXCR4 in primary human T cells and hematopoietic stem and progenitor cells using base editing. *Mol. Ther.* **30**, 130–144 (2022).
28. Li, S., Holguin, L. & Burnett, J. C. CRISPR-Cas9-mediated gene disruption of endogenous co-receptors confers broad resistance to HIV-1 in human primary cells and humanized mice. *Mol. Ther. Methods in Clin. Dev.* **24**, 321–331 (2022).
29. Stranford, D. M., Hung, M. E., Gargus, E. S., Shah, R. N. & Leonard, J. N. A systematic evaluation of factors affecting extracellular vesicle uptake by breast cancer cells. *Tissue Eng. Part A* **23**, 1274–1282 (2017).
30. Longatti, A. et al. High affinity single-chain variable fragments are specific and versatile targeting motifs for extracellular vesicles. *Nanoscale* **10**, 14230–14244 (2018).
31. Wang, J. H. et al. Anti-HER2 scFv-directed extracellular vesicle-mediated mRNA-based gene delivery inhibits growth of HER2-positive human breast tumor xenografts by prodrug activation. *Mol. Cancer Ther.* **17**, 1133–1142 (2018).
32. Kooijmans, S. A. et al. Display of GPI-anchored anti-EGFR nanobodies on extracellular vesicles promotes tumour cell targeting. *J. Extracell. Vesicles* **5**, 31053 (2016).
33. Connelly, R. J. et al. Mitogenic properties of a bispecific single-chain Fv-–Ig fusion generated from CD2-specific mAb to distinct epitopes. *Int. Immunol.* **10**, 1863–1872 (1998).
34. Telerman, A. et al. Internalization of human T lymphocyte receptors. *Eur. J. Immunol.* **17**, 991–997 (1987).
35. Chang, Z. L. et al. Rewiring T-cell responses to soluble factors with chimeric antigen receptors. *Nat. Chem. Biol.* **14**, 317–324 (2018).
36. Thery, C., Amigorena, S., Raposo, G. & Clayton, A. Isolation and characterization of exosomes from cell culture supernatants and biological fluids. *Curr. Protoc. Cell Biol.* **Chapter 3**, Unit 3.22 (2006).
37. Jeppesen, D. K. et al. Comparative analysis of discrete exosome fractions obtained by differential centrifugation. *J. Extracell. Vesicles* **3**, 25011 (2014).
38. Verweij, F. J. et al. The power of imaging to understand extracellular vesicle biology in vivo. *Nat. Methods* **18**, 1013–1026 (2021).
39. Simonsen, J. B. Pitfalls associated with lipophilic fluorophore staining of extracellular vesicles for uptake studies. *J. Extracell. Vesicles* **8**, 1582237 (2019).
40. Hung, M. E. & Leonard, J. N. A platform for actively loading cargo RNA to elucidate limiting steps in EV-mediated delivery. *J. Extracell. Vesicles* **5**, 31027 (2016).
41. Bu, J. et al. An avidity-based PD-L1 antagonist using nanoparticle–antibody conjugates for enhanced immunotherapy. *Nano Lett.* **20**, 4901–4909 (2020).
42. Raab, D., Graf, M., Notka, F., Schödl, T. & Wagner, R. The GeneOptimizer Algorithm: using a sliding window approach to cope with the vast sequence space in multiparameter DNA sequence optimization. *Syst. Synth. Biol.* **4**, 215–225 (2010).
43. Kooijmans, S. A. A., Gitz-Francois, J., Schiffelers, R. M. & Vader, P. Recombinant phosphatidylserine-binding nanobodies for targeting of extracellular vesicles to tumor cells: a plug-and-play approach. *Nanoscale* **10**, 2413–2426 (2018).
44. Yim, N. et al. Exosome engineering for efficient intracellular delivery of soluble proteins using optically reversible protein–protein interaction module. *Nat. Commun.* **7**, 12277 (2016).
45. Heath, N. et al. Endosomal escape enhancing compounds facilitate functional delivery of extracellular vesicle cargo. *Nanomedicine* **14**, 2799–2814 (2019).
46. Putyrski, M. & Schultz, C. Protein translocation as a tool: the current rapamycin story. *FEBS Lett.* **586**, 2097–2105 (2012).
47. Gao, Y. et al. Complex transcriptional modulation with orthogonal and inducible dCas9 regulators. *Nat. Methods* **13**, 1043–1049 (2016).
48. Maggio, I. et al. Integrating gene delivery and gene-editing technologies by adenoviral vector transfer of optimized CRISPR–Cas9 components. *Gene Ther.* **27**, 209–225 (2020).
49. de Jong, O. G. et al. A CRISPR–Cas9-based reporter system for single-cell detection of extracellular vesicle-mediated functional transfer of RNA. *Nat. Commun.* **11**, 1113 (2020).
50. Hung, M. E., Lenzini, S. B., Stranford, D. M. & Leonard, J. N. Enrichment of extracellular vesicle subpopulations via affinity chromatography. *Methods Mol. Biol.* **1740**, 109–124 (2018).
51. Somiya, M. & Kuroda, S. Real-time luminescence assay for cytoplasmic cargo delivery of extracellular vesicles. *Anal. Chem.* **93**, 5612–5620 (2021).
52. Mangeot, P. E. et al. Protein transfer into human cells by VSV-G-induced nanovesicles. *Mol. Ther.* **19**, 1656–1666 (2011).
53. Cronin, J., Zhang, X.-Y. & Reiser, J. Altering the tropism of lentiviral vectors through pseudotyping. *Curr. Gene Ther.* **5**, 387–398 (2005).
54. Frecha, C. et al. Stable transduction of quiescent T cells without induction of cycle progression by a novel lentiviral vector pseudotyped with measles virus glycoproteins. *Blood* **112**, 4843–4852 (2008).
55. Frecha, C. et al. Measles virus glycoprotein-pseudotyped lentiviral vector-mediated gene transfer into quiescent lymphocytes requires binding to both SLAM and CD46 entry receptors. *J. Virol.* **85**, 5975–5985 (2011).
56. Karampetsou, M. P., Comte, D., Kis-Toth, K., Kyttaris, V. C. & Tsokos, G. C. Expression patterns of signaling lymphocytic activation molecule family members in peripheral blood mononuclear cell subsets in patients with systemic lupus erythematosus. *PLoS ONE* **12**, e0186073 (2017).
57. Hashiguchi, T., Maenaka, K. & Yanagi, Y. Measles virus hemagglutinin: structural insights into cell entry and measles vaccine. *Front. Microbiol.* **2**, 247 (2011).
58. Gonçalves-Carneiro, D., McKeating, J. A. & Bailey, D. The measles virus receptor SLAMF1 can mediate particle endocytosis. *J. Virol.* **91**, e02255-16 (2017).
59. Soares, A. R. et al. Gap junctional protein Cx43 is involved in the communication between extracellular vesicles and mammalian cells. *Sci. Rep.* **5**, 13243 (2015).
60. Schumann, K. et al. Generation of knock-in primary human T cells using Cas9 ribonucleoproteins. *Proc. Natl Acad. Sci. USA* **112**, 10437–10442 (2015).

61. Hultquist, J. F. et al. A Cas9 ribonucleoprotein platform for functional genetic studies of HIV–host interactions in primary human T cells. *Cell Rep.* **17**, 1438–1452 (2016).
62. Liu, S. et al. HIV-1 inhibition in cells with CXCR4 mutant genome created by CRISPR–Cas9 and piggyBac recombinant technologies. *Sci. Rep.* **8**, 8573 (2018).
63. Zhu, X. et al. Comprehensive toxicity and immunogenicity studies reveal minimal effects in mice following sustained dosing of extracellular vesicles derived from HEK293T cells. *J. Extracell. Vesicles* **6**, 1324730 (2017).
64. Hultquist, J. F. et al. CRISPR–Cas9 genome engineering of primary CD4(+) T cells for the interrogation of HIV–host factor interactions. *Nat. Protoc.* **14**, 1–27 (2019).
65. Modarai, S. R., Kanda, S., Bloh, K., Opdenaker, L. M. & Kmiec, E. B. Precise and error-prone CRISPR-directed gene editing activity in human CD34$^+$ cells varies widely among patient samples. *Gene Ther.* **28**, 105–113 (2021).
66. Breuer, C. B. et al. In vivo engineering of lymphocytes after systemic exosome-associated AAV delivery. *Sci. Rep.* **10**, 4544 (2020).
67. Shrivastava, S. et al. Exosome-mediated stable epigenetic repression of HIV-1. *Nat. Commun.* **12**, 5541 (2021).
68. Cheng, Q. et al. Reprogramming exosomes as nanoscale controllers of cellular immunity. *J. Am. Chem. Soc.* **140**, 16413–16417 (2018).
69. Campbell, L. A. et al. Gesicle-mediated delivery of CRISPR/Cas9 ribonucleoprotein complex for inactivating the HIV provirus. *Mol. Ther.* **27**, 151–163 (2019).
70. Sterzenbach, U. et al. Engineered exosomes as vehicles for biologically active proteins. *Mol. Ther.* **25**, 1269–1278 (2017).
71. Dooley, K. et al. A versatile platform for generating engineered extracellular vesicles with defined therapeutic properties. *Mol. Ther.* **29**, 1729–1743 (2021).
72. Levy, C. et al. Lentiviral vectors displaying modified measles virus gp overcome pre-existing immunity in in vivo-like transduction of human T and B cells. *Mol. Ther.* **20**, 1699–1712 (2012).
73. Hendel, A. et al. Chemically modified guide RNAs enhance CRISPR–Cas genome editing in human primary cells. *Nat. Biotechnol.* **33**, 985–989 (2015).
74. Cornu, T. I., Mussolino, C., Bloom, K. & Cathomen, T. Editing CCR5: a novel approach to HIV gene therapy. *Adv. Exp. Med. Biol.* **848**, 117–130 (2015).
75. Zou, X. et al. Extracellular vesicles expressing a single-chain variable fragment of an HIV-1 specific antibody selectively target Env(+) tissues. *Theranostics* **9**, 5657–5671 (2019).
76. Wang, S., Beattie, G. M., Hayek, A. & Levine, F. Development of a VSV-G protein pseudotyped retroviral vector system expressing dominant oncogenes from a lacO-modified inducible LTR promoter. *Gene* **182**, 145–150 (1996).
77. Yoshida, Y., Emi, N. & Hamada, H. VSV-G-pseudotyped retroviral packaging through adenovirus-mediated inducible gene expression. *Biochem. Biophys. Res. Commun.* **232**, 379–382 (1997).
78. Sanjana, N. E., Shalem, O. & Zhang, F. Improved vectors and genome-wide libraries for CRISPR screening. *Nat. Methods* **11**, 783–784 (2014).
79. Ai, H. W., Shaner, N. C., Cheng, Z., Tsien, R. Y. & Campbell, R. E. Exploration of new chromophore structures leads to the identification of improved blue fluorescent proteins. *Biochemistry* **46**, 5904–5910 (2007).
80. Daringer, N. M., Dudek, R. M., Schwarz, K. A. & Leonard, J. N. Modular extracellular sensor architecture for engineering mammalian cell-based devices. *ACS Synth. Biol.* **3**, 892–902 (2014).
81. Atasoy, D., Aponte, Y., Su, H. H. & Sternson, S. M. A FLEX switch targets Channelrhodopsin-2 to multiple cell types for imaging and long-range circuit mapping. *J. Neurosci.* **28**, 7025–7030 (2008).
82. Heredia, J. D. et al. Mapping interaction sites on human chemokine receptors by deep mutational scanning. *J. Immunol.* **200**, 3825–3839 (2018).
83. Shen, Y., Rosendale, M., Campbell, R. E. & Perrais, D. pHuji, a pH-sensitive red fluorescent protein for imaging of exo- and endocytosis. *J. Cell Biol.* **207**, 419–432 (2014).
84. Cong, L. et al. Multiplex genome engineering using CRISPR/Cas systems. *Science* **339**, 819–823 (2013).
85. Anders, C. & Jinek, M. In vitro enzymology of Cas9. *Methods Enzymol.* **546**, 1–20 (2014).

Acknowledgements

We thank R. D'Aquila for his support and guidance in starting this project. We thank I. Clerc for her assistance with the measles virus glycoproteins. J.N.L. discloses support for the research described in this study from Third Coast Center for AIDS Research, an NIH-funded centre (P30 AI117943), NIH grants R01AI165236 and R01AI150998 (J.F.H.), National Science Foundation (NSF) award 1844219 (J.N.L. and N. P. Kamat), Kairos Ventures (gift), and Syenex. This work was also supported by NSF Graduate Research Fellowship awards DGE-1324585 (to D.M.S.) and DGE-1842165 (to B.N.D.). Sanger sequencing was performed through the Northwestern University Sequencing Core (NUSeq) Core Facility of Northwestern's Center for Genetic Medicine and a partnership with ACGT. NanoSight analysis was performed in the Analytical bioNanoTechnology Core Facility (ANTEC) of the Simpson Querrey Institute at Northwestern University. ANTEC is currently supported by the Soft and Hybrid Nanotechnology Experimental Resource (NSFECCS-1542205). We thank C. Wilke for her assistance with TEM. TEM was performed at the BioCryo facility of Northwestern University's Atomic and Nanoscale Characterization Experimental (NU*ANCE*) Center, which has received support from the Soft and Hybrid Nanotechnology Experimental Resource (NSF ECCS-1542205); the Materials Research Science and Engineering Centers (MRSEC) program (NSF DMR-1720139) at the Materials Research Center; the International Institute for Nanotechnology; and the State of Illinois, through the International Institute for Nanotechnology. It also made use of the CryoCluster equipment, which has received support from the Major Research Instrumentation (MRI) program (NSF DMR-1229693). We thank H. Edelstein for her assistance with confocal microscopy. Microscopy was performed at the Biological Imaging Facility at Northwestern University (RRID:SCR_017767), graciously supported by the Chemistry for Life Processes Institute, the Northwestern University Office for Research, and the Department of Molecular Biosciences. We thank P. Mehl for his assistance with FACS. Flow cytometry was performed at the Northwestern University Robert H. Lurie Comprehensive Cancer Center (RHLCCC) Flow Cytometry Facility, which is supported by a Cancer Center Support Grant (NCI CA060553). We thank J. Brink and S. Hockema at 496code for their assistance with HTS data analysis.

Author contributions

D.M.S. and J.N.L. conceptualized the project and designed the experiments. D.M.S., B.N.D. and M.E.H. performed the experiments. D.M.S. and J.N.L. analysed the data. L.M.S. isolated, activated, and electroporated the primary T cells. K.E.B. and L.C. conducted the MiSeq runs. D.M.S. drafted the original manuscript and created the figures. J.N.L., J.F.H. and J.B.L. supervised the work. All authors reviewed, edited, and approved the final manuscript.

Competing interests

J.N.L. and D.M.S. are co-inventors on patent pending intellectual property that covers some technologies reported in this manuscript. J.N.L. and D.M.S. have financial interest in Syenex, which could potentially benefit from the outcomes of this research.

Additional information

Extended data is available for this paper at https://doi.org/10.1038/s41551-023-01142-x.

Supplementary information The online version contains supplementary material available at https://doi.org/10.1038/s41551-023-01142-x.

Correspondence and requests for materials should be addressed to Joshua N. Leonard.

Peer review information *Nature Biomedical Engineering* thanks the anonymous reviewer(s) for their contribution to the peer review of this work.

https://doi.org/10.1038/s41551-023-01142-x

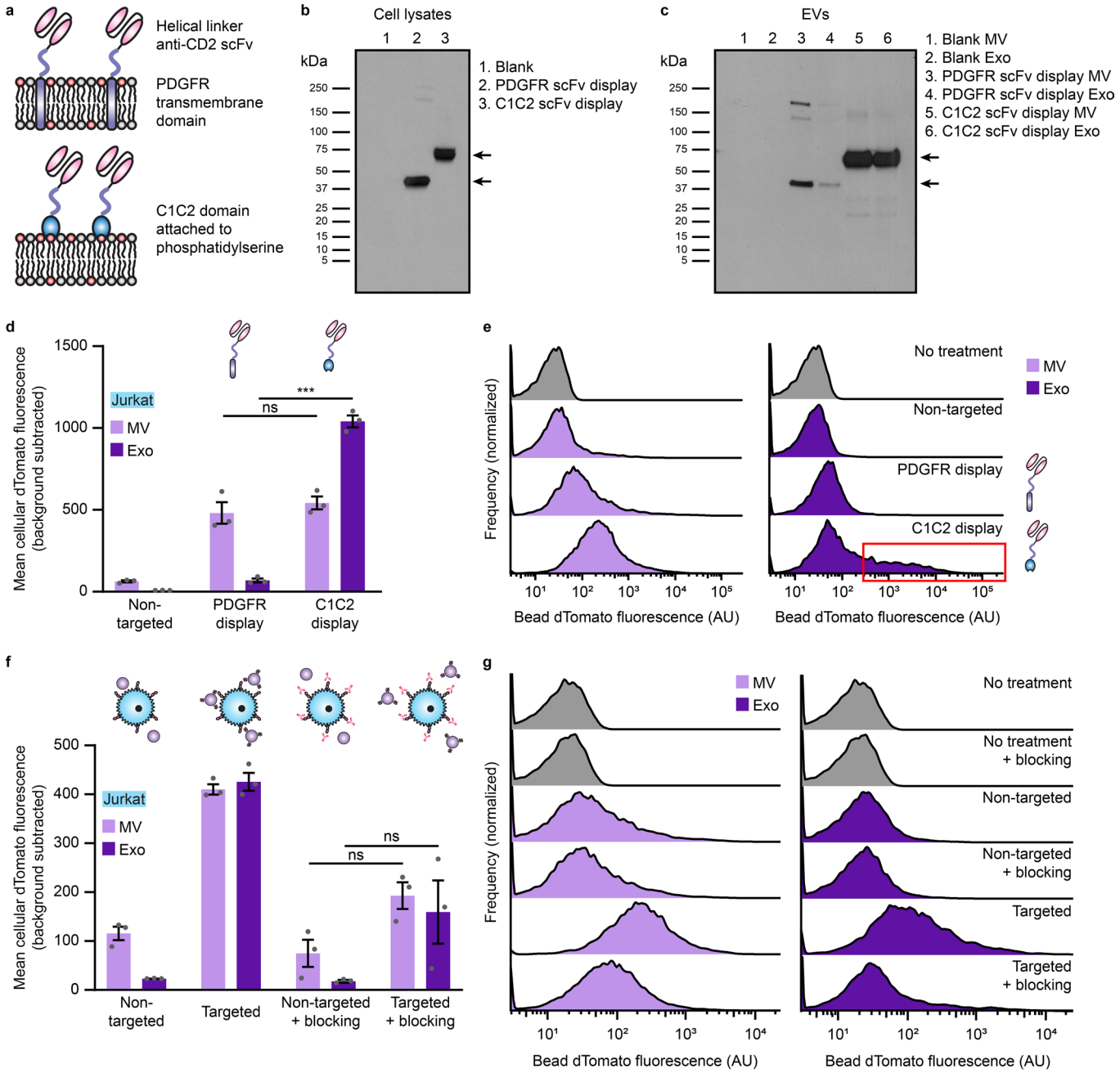

Extended Data Fig. 1 | Different scFv display techniques result in different EV targeting properties. a, Cartoon highlighting the structures of the PDGFR transmembrane domain scFv display and lactadherin C1C2 domain anchoring to phosphatidylserine. **b**, Expression of scFv constructs in EV producer cell lysates. 1 µg cell lysate was loaded per lane. Expected band sizes: ~40 kDa and ~75 kDa (black arrows). **c**, Loading of scFv constructs into EVs generated from cell lines in **b**. 5.0×10^8 EVs were loaded per lane. **d**, Binding of targeted EVs to Jurkat T cells following a 2 h incubation. **e**, Representative histograms corresponding to the summary data reported in **d**. The subpopulation of cells showing a skewed, high degree of exosome binding is indicated by the red box. **f**, Recipient Jurkat T cells were incubated for 1 h in the presence or absence of anti-CD2 antibodies prior to a 2 h incubation with EVs. **g**, Representative histograms corresponding to the summary data reported in **f**. Flow cytometry experiments were performed in biological triplicate, and error bars (panels **d**, **f**) indicate standard error of the mean. EV dTomato loading evaluations are presented in Supplementary Fig. 5. Statistical tests comprise two-tailed Student's t-tests using the Benjamini-Hochberg method to reduce the false discovery rate. (*$p < 0.05$, **$p < 0.01$, ***$p < 0.001$). Exact p-values are reported in Supplementary Table 1.

https://doi.org/10.1038/s41551-023-01142-x

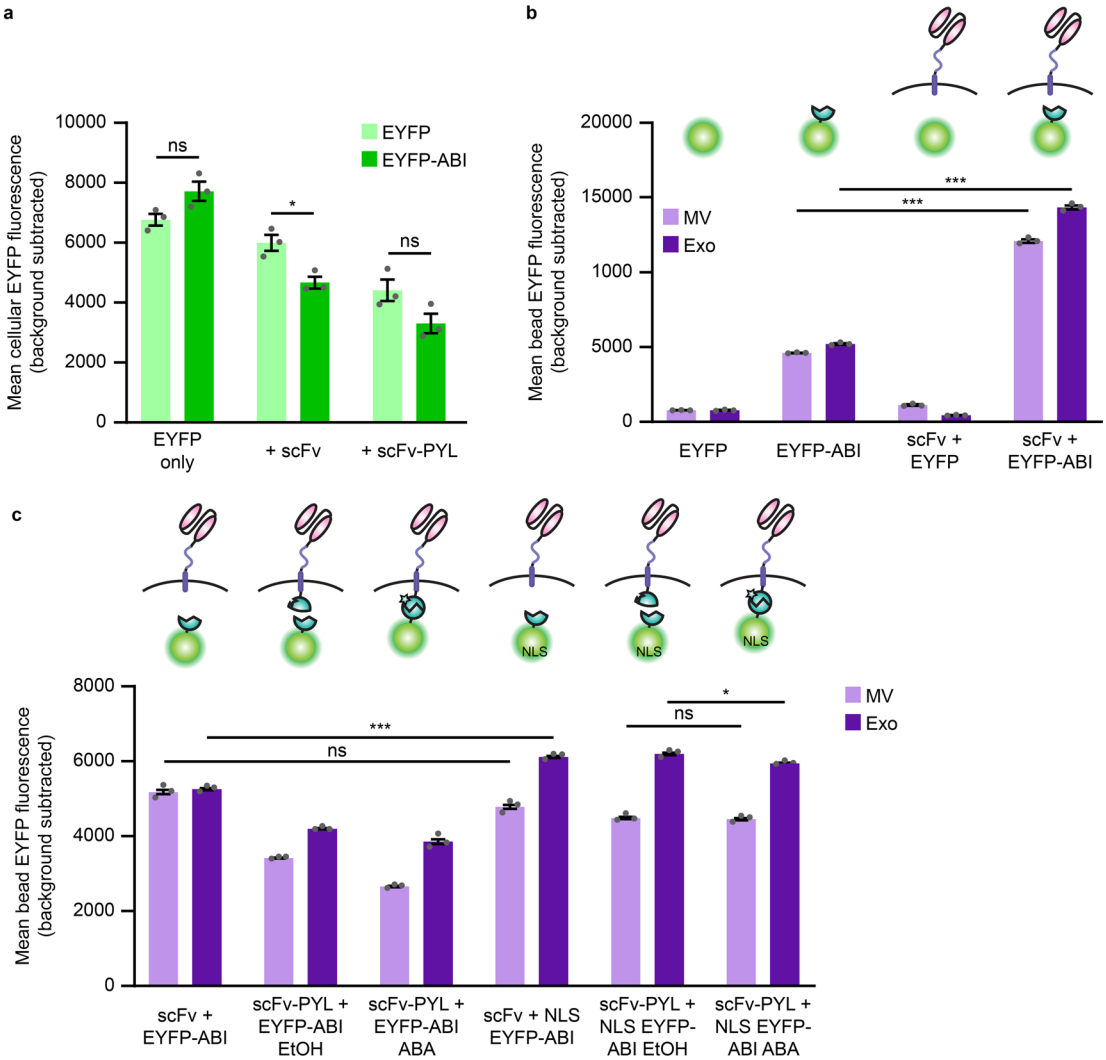

Extended Data Fig. 2 | The ABI domain increases EV-cargo loading independently of total protein expression. a, Expression of EYFP and EYFP-ABI in the presence of anti-CD2 targeting constructs in transiently transfected HEK293FT cells analysed by flow cytometry. A key observation is that addition of the ABI domain does not increase overall cargo protein expression in producer cells. **b**, Repeat of EYFP-ABI EV loading trends in the presence of an scFv shown in Fig. 3c. **c**, Comparison of EYFP loading into EVs with and without an NLS with ABA-binding constructs and under ABA-induced dimerization conditions. Addition of an NLS did not substantially impact EYFP loading, nor did ABA-induced dimerization substantially impact loading of nuclear-localized cargo. Experiments were performed in biological triplicate, and error bars indicate standard error of the mean. Statistical tests comprise two-tailed Student's t-tests using the Benjamini-Hochberg method to reduce the false discovery rate. (*$p < 0.05$, **$p < 0.01$, ***$p < 0.001$). Exact p-values are reported in Supplementary Table 1.

https://doi.org/10.1038/s41551-023-01142-x

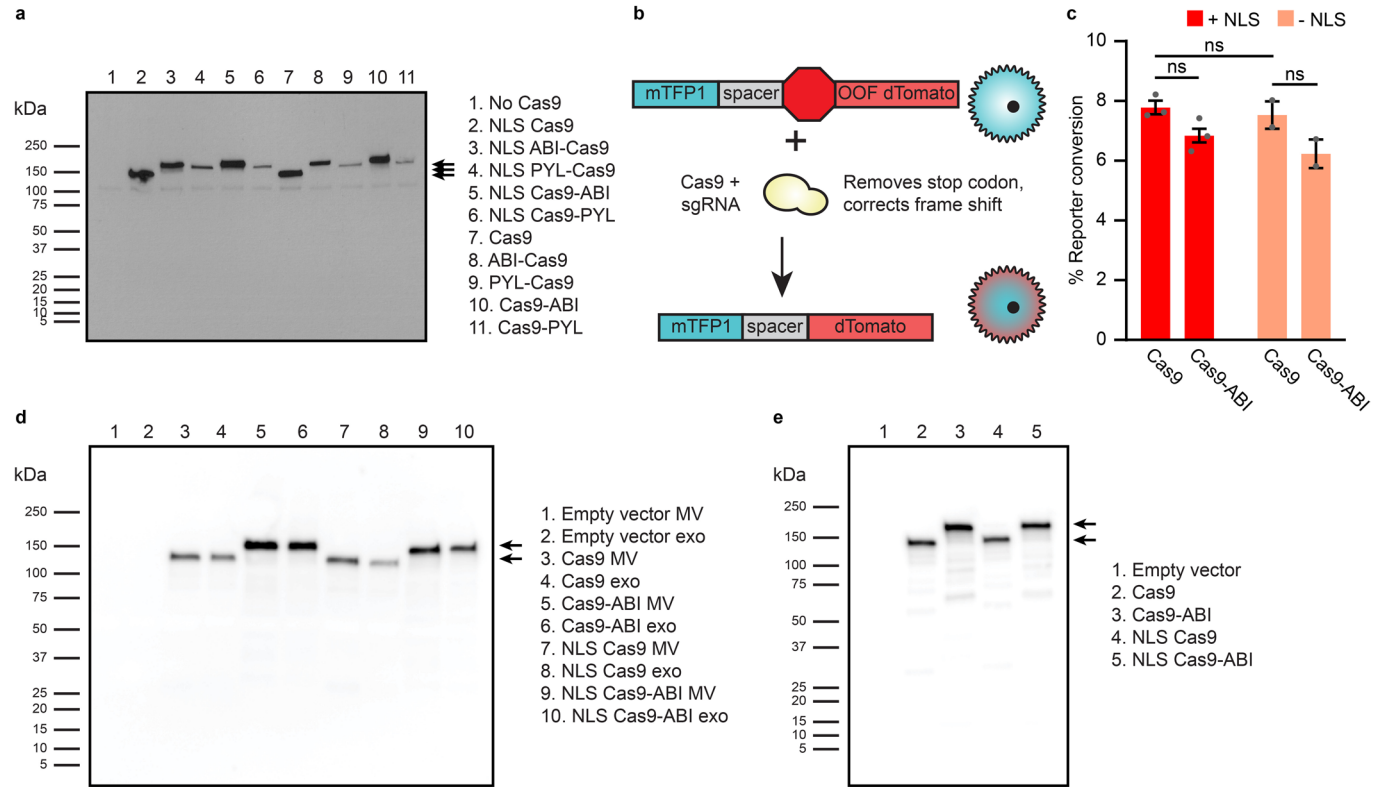

Extended Data Fig. 3 | The ABI domain increases Cas9 loading into EVs, and Cas9-ABI retains function. a, Expression of Cas9 fused to either the ABI or PYL domain in transiently transfected HEK293FT cells. 2 µg cell lysate was loaded per lane. Expected band sizes: ~160, 183, and 195 kDa (arrows). **b**, Cartoon illustrating the Cas9 reporter construct. Successful editing by Cas9 results in the deletion of a stop codon and (in some random fraction of cases) a repair-mediated frame shift induces express dTomato. **c**, Absence of an NLS or presence of the ABI domain does not meaningfully reduce Cas9 editing efficiency in transiently transfected Jurkat T cells. Cells were analysed by flow cytometry 3 d post-transfection. Experiments were performed in biological triplicate, and error bars indicate standard error of the mean. Statistical tests comprise two-tailed Student's t-tests using the Benjamini-Hochberg method to reduce the false discovery rate. (*$p < 0.05$, **$p < 0.01$, ***$p < 0.001$). Exact p-values are reported in Supplementary Table 1. Samples with high cellular autofluorescence were excluded from analysis. **d**, Full blot of Cas9 EV active loading data presented in Fig. 3e. **e**, Cellular expression of Cas9 with and without the ABI domain or an NLS. 2 µg cell lysate was loaded per lane.

https://doi.org/10.1038/s41551-023-01142-x

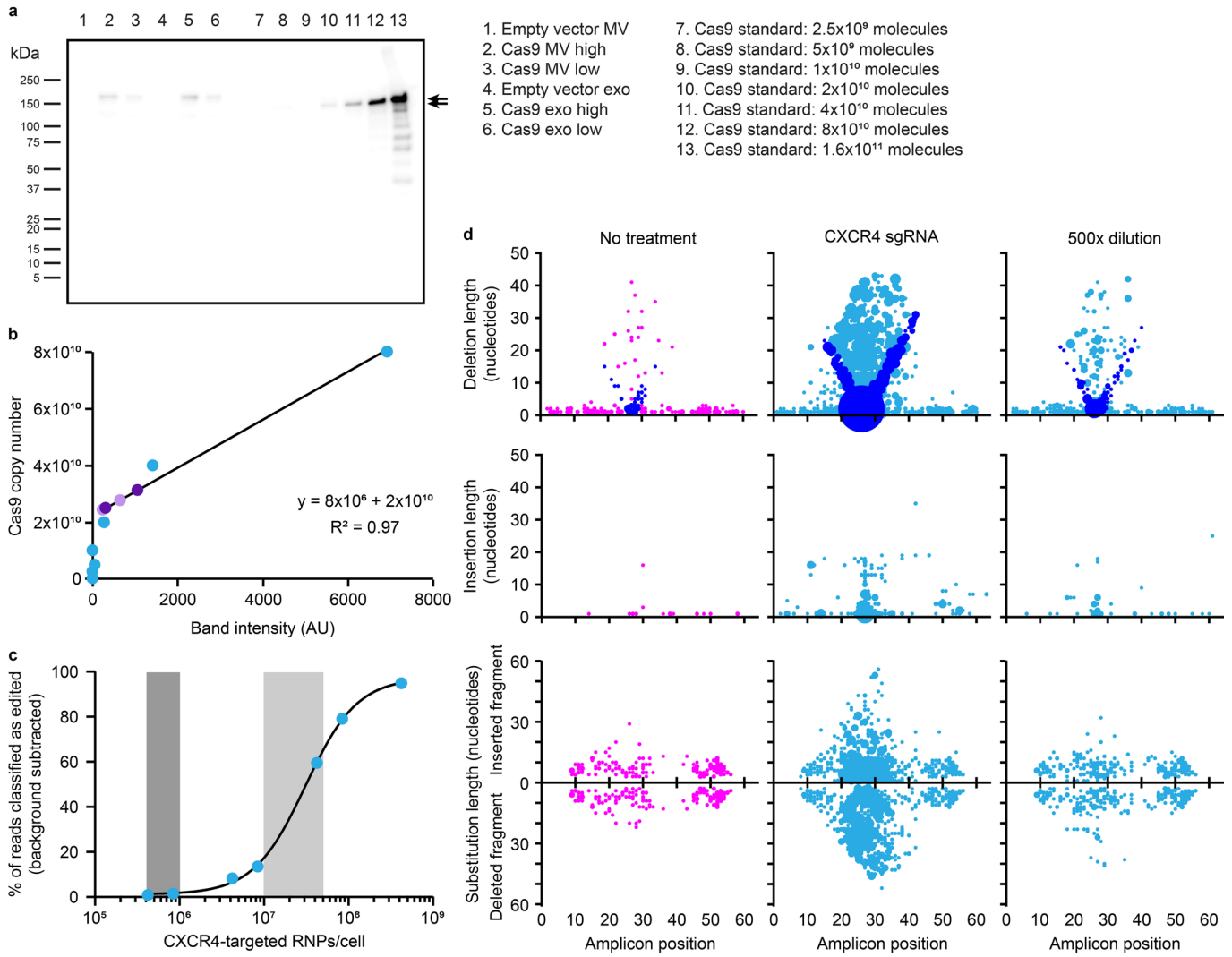

Extended Data Fig. 4 | Electroporation of recombinant Cas9-sgRNA ribonucleoprotein complexes into primary T cells confers dose-dependent editing of the genomic CXCR4 target locus. a, Analysis of actively loaded Cas9 molecules per EV in vesicles displaying an anti-CD2 scFv and VSV-G. Lanes loaded with 4.0×10^8 ('high') or 2.0×10^8 ('low') EVs were compared to samples loaded with specified numbers of recombinant Cas9 molecules quantified based upon the manufacturer's analysis (lanes 7-13). Expected band sizes (~160 or 195 kDa, arrows) correspond to Cas9 +/- the ABI domain. **b**, Quantification of Cas9 RNPs per EV. Band intensities from Cas9 standards in **a** were plotted against Cas9 molecules loaded (blue points), and loading of Cas9 into EVs was calculated using a line fit to the linear regime of the recombinant Cas9 standard curve (purple points; light: MV, dark: exo); this analysis indicates a loading of ~100 Cas9 molecules per EV. **c**, Frequency of indels detected at the Cas9-targeted CXCR4 locus after electroporation of $CD4^+$ T cells with different doses of CXCR4-targeted RNPs. Doses of recombinant Cas9 that correspond to equivalent Cas9 molecules per cell as EV delivery and equivalent Cas9 editing efficiencies as EVs are highlighted in light and dark grey, respectively. Background subtraction was performed using an untreated control; treatment of T cells with RNPs complexed with a non-targeted sgRNA produces similar levels of apparent CXCR4 editing as did the untreated controls, likely indicating that these conditions both represent noise associated with this assay. **d**, Distributions of RNP-mediated edits, by type, as described in Fig. 5. The no treatment, non-diluted CXCR4 sgRNA treatment (maximum editing), and 500x sgRNA dilution (similar editing frequency as EV-mediated delivery of Cas9-sgRNA) conditions are shown.

nature portfolio

Corresponding author(s): Joshua N. Leonard

Last updated by author(s): Oct 19, 2023

Reporting Summary

Nature Portfolio wishes to improve the reproducibility of the work that we publish. This form provides structure for consistency and transparency in reporting. For further information on Nature Portfolio policies, see our Editorial Policies and the Editorial Policy Checklist.

Statistics

For all statistical analyses, confirm that the following items are present in the figure legend, table legend, main text, or Methods section.

n/a	Confirmed
☐	☒ The exact sample size (*n*) for each experimental group/condition, given as a discrete number and unit of measurement
☐	☒ A statement on whether measurements were taken from distinct samples or whether the same sample was measured repeatedly
☐	☒ The statistical test(s) used AND whether they are one- or two-sided *Only common tests should be described solely by name; describe more complex techniques in the Methods section.*
☒	☐ A description of all covariates tested
☐	☒ A description of any assumptions or corrections, such as tests of normality and adjustment for multiple comparisons
☐	☒ A full description of the statistical parameters including central tendency (e.g. means) or other basic estimates (e.g. regression coefficient) AND variation (e.g. standard deviation) or associated estimates of uncertainty (e.g. confidence intervals)
☐	☒ For null hypothesis testing, the test statistic (e.g. *F*, *t*, *r*) with confidence intervals, effect sizes, degrees of freedom and *P* value noted *Give P values as exact values whenever suitable.*
☒	☐ For Bayesian analysis, information on the choice of priors and Markov chain Monte Carlo settings
☒	☐ For hierarchical and complex designs, identification of the appropriate level for tests and full reporting of outcomes
☒	☐ Estimates of effect sizes (e.g. Cohen's *d*, Pearson's *r*), indicating how they were calculated

Our web collection on statistics for biologists contains articles on many of the points above.

Software and code

Policy information about availability of computer code

Data collection	Flow-cytometry data were collected using BD FACS DIVA software. NanoSight data were collected using Malvern NTA software version 3.4. HTS data were collected on an Illumina MiSeq using MiSeq Control System v4.
Data analysis	Flow-cytometry data were analysed using FlowJo software v10. NanoSight data were analysed using Malvern NTA software version 3.4. Where indicated, microscopy images were analysed using ImageJ 1.53f51. Custom code for HTS analysis will be available on GitHub along with the final published version of the manuscript. Graphs were generated and statistical analyses were performed using Microsoft Excel 365 and GraphPad Prism 9.3.0. Figures were compiled using Adobe Illustrator 2022. The code for analysing the high-throghput screening data is available at https://github.com/leonardlab/GEMINI-HTS under an open-source license.

For manuscripts utilizing custom algorithms or software that are central to the research but not yet described in published literature, software must be made available to editors and reviewers. We strongly encourage code deposition in a community repository (e.g. GitHub). See the Nature Portfolio guidelines for submitting code & software for further information.

Data

Policy information about availability of data

All manuscripts must include a data availability statement. This statement should provide the following information, where applicable:

- Accession codes, unique identifiers, or web links for publicly available datasets
- A description of any restrictions on data availability
- For clinical datasets or third party data, please ensure that the statement adheres to our policy

All reported experimental data and plasmid maps for all plasmids generated in this study are freely available at Zenodo (https://doi.org:10.5281/zenodo.10022991). Key plasmids used in this study are distributed by Addgene, with complete and annotated GenBank files available at https://www.addgene.org/Joshua_Leonard. The raw and analysed datasets generated during the study are available for research purposes from the corresponding author on reasonable request.

Field-specific reporting

Please select the one below that is the best fit for your research. If you are not sure, read the appropriate sections before making your selection.

☒ Life sciences ☐ Behavioural & social sciences ☐ Ecological, evolutionary & environmental sciences

For a reference copy of the document with all sections, see nature.com/documents/nr-reporting-summary-flat.pdf

Life sciences study design

All studies must disclose on these points even when the disclosure is negative.

Sample size	All experiments were conducted in biological triplicates, which is standard for this type of study.
Data exclusions	In one experiment, some sample replicates were excluded owing to the unnaturally high cellular autofluorescence observed during flow cytometry. This is noted in the appropriate source-data file.
Replication	For many of the experiments performed, similar samples or conditions were included across multiple experiments to validate repeatability (for example, T-cell binding by CD2-targeted vesicles was validated across several independent experiments investigating aspects of that binding). In some cases, such as in certain high-throughput-screening experiments, the conditions were repeated using independent vesicle preparations and donor cells, to confirm trends and repeatability.
Randomization	Randomization was not relevant to the study.
Blinding	Blinding was not relevant to the study, as no conclusions were based on subjective analysis.

Reporting for specific materials, systems and methods

We require information from authors about some types of materials, experimental systems and methods used in many studies. Here, indicate whether each material, system or method listed is relevant to your study. If you are not sure if a list item applies to your research, read the appropriate section before selecting a response.

Materials & experimental systems

n/a	Involved in the study
☐	☒ Antibodies
☐	☒ Eukaryotic cell lines
☒	☐ Palaeontology and archaeology
☒	☐ Animals and other organisms
☒	☐ Human research participants
☒	☐ Clinical data
☒	☐ Dual use research of concern

Methods

n/a	Involved in the study
☒	☐ ChIP-seq
☐	☒ Flow cytometry
☒	☐ MRI-based neuroimaging

Antibodies

Antibodies used	anti-FLAG, Sigma F1804, diluted 1:1000 anti-HA, Cell Signaling Technology 377245 C29F4, diluted 1:1000 anti-CD9, Santa Cruz Biotechnology sc-13118, diluted 1:500 anti-CD81, Santa Cruz Biotechnology sc-23962, diluted 1:500 anti-Alix, Abcam Ab117600, diluted 1:500 anti-calnexin, Abcam Ab22595, diluted 1:1000 HRP-conjugated anti-mouse, Cell Signaling Technology 7076, diluted 1:3000

HRP-conjugated anti-rabbit, Invitrogen 32460, diluted 1:3000
anti-FLAG-APC, Abcam Ab72569 at manufacturer recommended dose
anti-CD2-APC, R&D Systems FAB18561A at manufacturer recommended dose
anti-CD25-PE, Miltenyi REA945, 130-115-628 at manufacturer recommended dose
anti-SLAM-PE, Miltenyi REA151, 130-123-970 at manufacturer recommended dose
anti-mouse IgG1-APC R&D Systems IC002A at manufacturer recommended dose
anti-human IgG1-PE, Miltenyi REA293, 130-113-438 at manufacturer recommended dose
anti-CD2-APC, Beckman Coulter A60794 at manufacturer recommended dose
anti-Cas9, Cell Signaling Technology 7A9-3A3, diluted 1:1000

Validation

From Sigma: "Our standard antibody validation processes include verification for each recommended immunodetection application. Each of the thousands of antibodies in our portfolio are certified through our standard validation process to ensure quality and reproducibility."
From Cell Signaling Technology: "To ensure our antibodies will work in your experiment, we adhere to the Hallmarks of Antibody Validation™, six complementary strategies that can be used to determine the functionality, specificity, and sensitivity of an antibody in any given assay. CST adapted the work by Uhlen, et. al., ("A Proposal for Validation of Antibodies." Nature Methods (2016)) to build the Hallmarks of Antibody Validation, based on our decades of experience as an antibody manufacturer and our dedication to reproducible science."
From Abcam: "Antibody validation must be application-specific to be effective and information on which applications an antibody has been validated in can be found in the Tested Applications section on any antibody datasheet."
From Invitrogen: "Thermo Fisher Scientific is committed to adopting higher validation standards for the Invitrogen antibody portfolio. We have implemented additional specificity tests to help ensure the highest confidence levels in our products."
From R&D Systems: "R&D Systems® takes rigorous steps towards antibody validation and reproducibility. We have been since the beginning. For 30 years, we have used our industry-leading production standards and quality control specifications to develop antibodies that can be relied on for specificity and reproducibility. By developing and testing our products in-house, we can ensure a validated and specific antibody. We are confident in our antibodies and provide 100% guarantee for our products."
From Miltenyi: "All our antibodies are rigorously tested and validated before release. In the application section on the product page, you can find examples of typical performance data. In addition, we provide extended validation data highlighting details of antibody performance, specificity, and fixation compatibility."
From Beckman Coulter: "We develop and manufacture reagents according to current Good Manufacturing Practices (cGMP), the highest quality standards in the industry, ensuring optimal antibody panel performance."
Whenever possible, negative controls are included in the antibody experiments. For Western blots, this includes samples that do not contain the tag being detected. For flow cytometry, this includes cell lines lacking the antibody's target receptor or an appropriate isotype control.

Eukaryotic cell lines

Policy information about cell lines

Cell line source(s)

HEK293FT cells, Thermo Fisher R70007
Jurkat T cells, ATCC TIB-152
Other cell lines, which were derived from those above using lentiviral integration.

Authentication

The cell-line vendors perform routine authentication; no further authentication was performed.

Mycoplasma contamination

HEK293FT and Jurkat T cells tested negative for mycoplasma.

Commonly misidentified lines
(See ICLAC register)

No commonly misidentified cells were used.

Flow Cytometry

Plots

Confirm that:

☒ The axis labels state the marker and fluorochrome used (e.g. CD4-FITC).

☒ The axis scales are clearly visible. Include numbers along axes only for bottom left plot of group (a 'group' is an analysis of identical markers).

☐ All plots are contour plots with outliers or pseudocolor plots.

☐ A numerical value for number of cells or percentage (with statistics) is provided.

Methodology

Sample preparation

For EV-binding experiments, cells were incubated for 2 h at 37°C unless otherwise indicated, then washed three times in FACS buffer, centrifuging at 150 g for 5 min for Jurkat cells or 400 g for 3 min for primary T cells. Cells were resuspended in one drop of FACS buffer PBS (pH 7.4 with 2 mM EDTA and 0.05% BSA) prior to flow cytometry. For EV-uptake experiments, cells were washed twice in PBS and incubated with two drops of trypsin-EDTA for 5 min at 37°C to remove surface-bound vesicles. Cells were washed with RPMI to quench the trypsin, then washed twice more with FACS buffer prior to analysis. For surface immunoblotting, cells were washed one or three times post-staining with 1 mL of FACS buffer, centrifuging at 400 g for 3 min or 150 g for 5 min and decanting the supernatant after each wash. Cells were resuspended in two drops of FACS buffer prior to flow cytometry. Beads were diluted and analysed in PBS.

Instrument	Analytical flow cytometry was performed on a BD LSR Fortessa Special Order Research Product (Robert H. Lurie Cancer Center Flow Cytometry Core) using the 562-nm laser for dTomato (582/15 filter), the 488-nm laser for EYFP (530/30 filter), and the 488-nm and 405-nm lasers for mTFP1 (530/30 filter and 525/50 filter, respectively). FACS was performed on a BD FacsAria IIu (Robert H. Lurie Cancer Center Flow Cytometry Core) using a 488-nm laser for mTFP1 (530/30 filter) or a 562-nm laser for dTomato (582/15 filter).
Software	Data were analysed using FlowJo v10 (FlowJo, LLC).
Cell population abundance	Cells were sorted into a mTFP+ dTomato– population for Cas9 reporter experiments. Reporter construct expression was validated by analytical flow cytometry, where an average of 96.8% (stdev 0.2) of cells were classified as mTFP+ and 100% of cells were classified as dTomoto– prior to Cas9 addition.
Gating strategy	Live cells were identified by FSC-A vs. SSC-A gating, and single cells were then identified by FSC-A vs. FSC-H gating. Beads were identified by FSC-A vs. SSC-A gating. A fluorescent protein was used to identify transfected cells in relevant experiments. A sample transfected with an empty vector was used to draw a gate identifying transfected cells such that less than 1% of non-fluorescent cells were included in the analysis.

☒ Tick this box to confirm that a figure exemplifying the gating strategy is provided in the Supplementary Information.